

1 **Cross species multi-omics reveals cell wall sequestration and elevated global transcription**
2 **as mechanisms of boron tolerance in plants**

3

4 Guannan Wang¹, Sandra Feuer DiTusa¹, Dong-Ha Oh¹, Achim D. Herrmann², David G.
5 Mendoza-Cozatl³, Malcolm A. O'Neill⁴, Aaron P. Smith¹, and Maheshi Dassanayake¹✉

6 ¹Department of Biological Sciences, Louisiana State University, Baton Rouge, LA, USA

7 ²Department of Geology & Geophysics and Coastal Studies Institute, Louisiana State University,
8 Baton Rouge, LA, USA

9 ³Division of Plant Sciences, Interdisciplinary Plant Group, Christopher S. Bond Life Sciences
10 Center, University of Missouri, Columbia, MO, USA

11 ⁴Complex Carbohydrate Research Center, The University of Georgia, Athens, GA, USA

12 ✉ maheshid@lsu.edu

13

14 **Keyword:** *Schrenkiella parvula*, extremophyte, boron toxicity, boron tolerance, boron
15 transporters, cell wall, RNA metabolism, stress-preparedness

16

17

18 **Abstract**

19 Boron toxicity is a worldwide problem for crop production, yet we have only a limited
20 understanding of the genetic responses and adaptive mechanisms to this environmental stress in
21 plants. Here we identified responses to excess boron in boron stress-sensitive *Arabidopsis*
22 *thaliana* and its boron stress-tolerant extremophyte relative *Schrenkiella parvula* using
23 comparative genomics, transcriptomics, metabolomics, and ionomics. *S. parvula* maintains a
24 lower level of total boron and free boric acid in its roots and shoots and sustains growth for
25 longer durations than *A. thaliana* when grown with excess boron. *S. parvula* likely excludes
26 boron more efficiently than *A. thaliana*, which we propose is partly driven by BOR5, a boron
27 transporter that we functionally characterized in the current study. Both species allocate
28 significant transcriptomic and metabolomic resources to enable their cell walls to serve as a
29 partial sink for excess boron, particularly discernable in *A. thaliana* shoots. We provide evidence
30 that the *S. parvula* transcriptome is pre-adapted to boron toxicity, exhibiting substantial overlap
31 with the boron-stressed transcriptome of *A. thaliana*. Our transcriptomic and metabolomics data

32 also suggest that RNA metabolism is a primary target of boron toxicity. Cytoplasmic boric acid
33 likely forms complexes with ribose and ribose-containing compounds critical to RNA and other
34 primary metabolic functions. A model depicting some of the cellular responses that enable a
35 plant to grow in the presence of normally toxic levels of boron is presented.

36

37 Keywords: excess boron stress, transcriptome, ionome, metabolome, extremophyte, boron
38 transporter, *Schrenkiella parvula*

39

40 **Introduction**

41 In 1899 the eminent botanist Edwin Copeland stated that “boron produced monstrosity”
42 to describe plant damage due to excess boron (Copeland and Kahlenberg, 1899). Boron functions
43 as an essential micronutrient in plants at a narrow concentration range (0.5 - 1 ppm, equivalent to
44 46.2 - 92.5 μM in hydroponic media), causing severe growth defects in many plants, including
45 most crops, at only slightly higher concentrations (Brenchley, 1914; Haas, 1929; Warington,
46 1937; Eaton, 1940; Goldberg, 1997; Reid, 2007, 2013; Julkowska, 2018; Landi et al., 2019).
47 Early surveys of boron toxicity effects led plants to be classified as sensitive, semi-tolerant, or
48 tolerant to boron (Eaton, 1935). Subsequently, the Food and Agriculture Organization of the
49 United Nations recommended a soil boron level of less than 1.4 mM for even the most tolerant
50 crops to minimize losses in productivity (Eaton, 1944; Ayers and Westcot, 1985; Grieve et al.,
51 2011). The negative impact of boron toxicity on US agriculture was recognized early on (Cook
52 and Wilson, 1918; Eaton, 1935). It is also known to reduce crop yields on all continents where
53 agricultural regions are affected by naturally high amounts of boron in soils or in irrigation
54 water, particularly when the water is obtained from sources near active geothermal areas (Nable
55 et al., 1997; Camacho-cristóbal et al., 2008; Reid and Fitzpatrick, 2009b). Moreover, most soils
56 containing toxic levels of boron occur in semi-arid environments where drought and high salinity
57 compound the stresses on the crops (Reid, 2010).

58 Excess boron inhibits plant growth by decreasing chlorophyll content, stomatal
59 conductance, photosynthesis, and leads to premature death of shoots and roots (Lovatt and Bates,
60 1984; Reid et al., 2004; Miwa et al., 2007). Nevertheless, the molecular targets of excess boron
61 and the cellular and molecular processes interrupted by boron stress are poorly understood.
62 Similarly, we have little understanding of the genetic mechanisms underlying boron toxicity

63 responses or the adaptive mechanisms plants use to counter excess boron (Reid et al., 2004; Ruiz
64 et al., 2003; Princi et al., 2016).

65 In this study, we used the boron-tolerant extremophyte *Schrenkiella parvula* (formerly
66 *Thellungiella parvula* and *Eutrema parvulum*, family Brassicaceae) (Dassanayake et al., 2011;
67 Zhu, 2015; Kazachkova et al., 2018) and its close relative *A. thaliana*, a boron-sensitive model,
68 to identify cellular processes interrupted by excess boron and to determine the transcriptional and
69 metabolic processes that support growth during boron toxicity. *S. parvula* is adapted to high
70 levels of boron naturally present in its native habitats in the Central Anatolian plateau of Turkey
71 (Helvacı et al., 2004). The ecotype (Lake Tuz) used in our study was collected from the Lake
72 Tuz region of Turkey and experiences an average concentration of boron (2.2 mM) that is highly
73 toxic to most plants (Nilhan et al., 2008). It can survive soil boron levels as high as 5.8 mM
74 boron in the wild (Nilhan et al., 2008) and 10 mM boron given for two weeks in controlled
75 environments (Oh et al., 2014). However, the mechanisms that allow *S. parvula* to grow in the
76 presence of boron concentrations that are toxic to *A. thaliana* are not known.

77 Here, we used comparative genomics, transcriptomics, ionomics, and metabolomics to
78 study boron toxicity responses and tolerance in *A. thaliana* and *S. parvula*. Our data suggest that
79 excess boron disturbs cell wall metabolism and RNA metabolism-related processes, particularly
80 translation. The cell walls of *A. thaliana* and *S. parvula* serve as a sink to partially sequester
81 excess boron under high boron conditions. *S. parvula* accumulated less boron than *A. thaliana*
82 under boron toxicity, likely through an efficient efflux system. We propose that *S. parvula* has a
83 pre-adapted transcriptome to facilitate rapid metabolic changes when exposed to excess boron
84 and that such a pre-adaptation distinguishes boron stress-adapted and -sensitive plants. We
85 provide a model depicting critical cellular processes that are affected by excess boron and the
86 molecular mechanisms boron stress-tolerant plants use to minimize the growth inhibitory effects
87 of this element.

88

89 **Results**

90 ***S. parvula* accumulates less boron while sustaining growth for longer durations compared**
91 **to *A. thaliana*.** *S. parvula* was unaffected by treatments of 5, 10, or 15 mM boric acid whether
92 grown hydroponically for four weeks (Figure 1A) or on plates for one week (Figure 1B). In
93 contrast, *A. thaliana* showed clear growth inhibition, wilting, and chlorosis of leaves 5 or 7 days

94 after the boric acid treatments (Figure 1A and B). The control growth media included ~100 μ M
95 boron to provide a boron-sufficient growth medium, and the treatments added excess boron to
96 this growth-sufficient level. We observed a substantial reduction in the fresh and dry weights of
97 *A. thaliana* shoots and roots in response to excess boron, whereas *S. parvula* biomass was
98 unaffected by the treatments (Figure 1C). Similarly, total chlorophyll content decreased in *A.*
99 *thaliana* but remained unchanged in *S. parvula* at 3 days after the treatments (Figure 1D). In *A.*
100 *thaliana*, we observed dose-dependent inhibitory effects of excess boron on root growth, whereas
101 *S. parvula* root growth was not affected (Figure 1E). In *A. thaliana*, the 15 mM boron treatment
102 led to a significant reduction of lateral root density (Figure 1F), while average lateral root length
103 was decreased in all treatments (Figure 1G). In contrast, neither lateral root density nor average
104 lateral root length of *S. parvula* was affected by excess boron (Figure 1F and G).

105 We quantified the concentration of boron (on a dry weight basis) in shoots and roots of
106 plants exposed to excess boron using inductively coupled plasma mass spectrometry (ICP-MS)
107 to determine if the distinct boron stress-responses between *S. parvula* and *A. thaliana* reflected
108 differences in their boron accumulation (Figure 1H). The initial boron levels in roots and shoots
109 of control plants were similar for both species. Differences in boron accumulation only differed
110 in response to the excess boron treatments. The levels of boron increased significantly in the
111 roots and shoots of both species over time and with higher concentrations of boron. However, the
112 level of boron that accumulated in *S. parvula* was lower than in *A. thaliana*. This was most
113 apparent in roots, 24 hours after the 5 mM boric acid treatment, in which boron levels increased
114 14-fold in *A. thaliana* but were unchanged in *S. parvula* (Figure 1H). The greater capacity of *S.*
115 *parvula* to maintain lower boron levels relative to *A. thaliana* may have contributed to the
116 continued root growth in *S. parvula* under conditions that decreased *A. thaliana* root growth
117 (Figure 1E). However, *S. parvula* roots could not limit boron accumulation comparable to
118 control plants when grown on 10 mM boric acid. Nevertheless, under this treatment, the relative
119 accumulation of boron in roots was still much lower in *S. parvula* than in *A. thaliana* (Figure
120 1H). In contrast to roots, *S. parvula* shoots significantly accumulated boron even within 3 hours
121 of the 5 mM boric acid treatment, although the amounts were lower than in *A. thaliana* shoots
122 under all comparable treatments (Figure 1H). This indicated that the overall response to excess
123 boron is different between roots and shoots.

124 We next determined if the physiological responses (Figure 1 A-G) to excess boron
125 coincided with a disruption in the ionic balance of other elements. Reduction of nutrient uptake
126 or concurrent over-accumulation of other elements may cause toxicity symptoms not directly
127 attributed to boron stress. To this end, we quantified 20 other elements known for their presence
128 in plants (Supplemental Figure 1). Neither species showed dramatic changes to their ionic
129 profiles during boron treatments except for the expected increase in boron content, suggesting
130 that the observed physiological responses in both species were largely caused by the cellular
131 disturbances due to excess boron accumulation.

132

133 **High external boron results in a substantial increase in free boric acid in *A. thaliana* roots**
134 **but not in *S. parvula* roots.** After being transported primarily as free boric acid into the
135 cytoplasm, boron is either found as free boric acid/borate or bound to organic metabolites within
136 plant cells (Woods, 1996; Hu and Brown, 1997; Brown et al., 2002; Broadley et al., 2012;
137 Camacho-cristóbal et al., 2008). We therefore measured the relative abundance of free boric acid
138 in plants using gas chromatography-mass spectrometry (GC-MS), to assess how *S. parvula* may
139 retain externally supplied boric acid differently from *A. thaliana* (Figure 1I). Notably, we
140 detected substantial increases (up to 14 fold) in free boric acid in treated *A. thaliana* shoots
141 compared to the control, which was comparable to the increase in total boron accumulation
142 (Figure 1H). In contrast, the increase in free boric acid (up to 4.5 fold, Figure 1I) was much
143 lower than the total boron accumulation in *A. thaliana* roots (Figure 1H). This suggested that a
144 major fraction of the increased total boron in *A. thaliana* roots was in the form of B-complexes.
145 *S. parvula* shoots were similar to *A. thaliana* roots since the increase in free boric acid (up to 2.2
146 fold; Figure 1I) was much lower than the increase of total boron in treated *S. parvula* shoots
147 (Figure 1H). It is equally noteworthy that the levels of free boric acid remained unchanged in *S.*
148 *parvula* roots under all conditions tested (Figure 1I) despite the substantial increases of total
149 boron in plants grown on 10 mM boric acid (Figure 1H). This led us to hypothesize that *S.*
150 *parvula* stores much of the excess boron in the form of B-complexes and thereby minimizes the
151 accumulation of free boric acid, particularly in roots, more effectively than *A. thaliana*.

152

153 **The transcriptomic response to excess boron is greater in *A. thaliana* than *S. parvula*.** We
154 expected that *A. thaliana* and *S. parvula*, which have rapid yet divergent responses to excess

155 boron, would exhibit regulation at the transcriptional level that determined their subsequent
156 responses to this stress. To develop a comparative framework to contrast transcriptional
157 responses to excess boron, plants were transferred to media containing 5 mM boric acid. This
158 concentration was sufficient to induce discernible changes in both species (Figure 1), but did not
159 cause tissue death in the sensitive model even at 5 days post treatment (Figure 1A). We chose a
160 24-hour duration to allow us to assess transcriptomic responses when neither species showed
161 observable changes to suggest cell death. Since the root stress response was different from that of
162 shoots, we investigated root and shoot transcriptomes separately in our comparative –omics
163 framework.

164 The largest observed variance (>40%) in the transcriptomes within a species was
165 attributed to the tissue differences (i.e. root versus shoot) as seen in the principal component
166 analysis (PCA) (Figure 2A). However, when we compared the transcriptomes of the same tissues
167 across species, the treated *A. thaliana* transcriptomes were strikingly different from the control,
168 whereas *S. parvula* treated and control transcriptomes were almost indistinguishable (Figure 2B).
169 This suggested that the extent of the transcriptional adjustment to excess boron is much greater
170 in *A. thaliana* than in *S. parvula*. Indeed, we found 9,657 genes in shoots and 6,126 genes in
171 roots differentially expressed in response to excess boron in *A. thaliana* (Supplemental Figure 2).
172 In contrast, the number of boron stress-responsive genes in *S. parvula* was much smaller (535 in
173 shoots and 63 in roots) (Supplemental Figure 2, Supplemental Data Set 1). The magnitude of the
174 differences in the overall transcriptomes reflected the visible physiological responses of these
175 two species to excess boron (Figure 1).

176 To independently assess the reproducibility of the transcriptomic responses captured by
177 RNAseq, we selected five to six differentially expressed genes per tissue in both species and
178 additional biological replicates to obtain the relative expression of 20 genes using RT-qPCR. We
179 found high concordance in transcript level changes between the RNAseq and RT-qPCR data
180 (Pearson $R^2 = 0.71$, $p = 2.65e-07$) (Supplemental Figure 3).

181

182 ***A. thaliana* and *S. parvula* exhibit differences in boron transporter gene expression and**
183 **function.** Boron uptake and translocation are known to involve a family of boron transporters
184 (BORs) and membrane intrinsic proteins (MIPs) (Diehn et al., 2019; Yoshinari and Takano,
185 2017). We compared the expression changes of all known boron transporters and channels to

186 determine the transcriptional responses to excess boron related to boron acquisition and transport
187 (Supplemental Data Set 1, Figure 2C, D). *S. parvula* roots showed down-regulation of both
188 *NIP5;1* and *BOR1*, the two dominant transporters mediating boron uptake and xylem loading
189 during boron-deficient conditions (Takano et al., 2002, 2006). *A. thaliana* roots also showed
190 down-regulation of *NIP5;1* (Figure 2C). This observation supports the idea that both species
191 attempted to reduce boron uptake as well as boron transport to the shoot in response to excess
192 boron.

193 Plants may alleviate boron toxicity by activating transporters that export boron back to
194 soil or to other compartments away from actively growing tissues, in addition to minimizing
195 boron uptake. *BOR4* is the only boron transporter demonstrated to alleviate boron toxicity by
196 moving excess boron from roots back to soil (Miwa et al., 2014, 2007). Our transcriptomic data
197 showed that *BOR4* transcript abundance was not affected by excess boron in either *A. thaliana* or
198 *S. parvula* (Figure 2C). However, basal transcript levels of *SpBOR4* were ~5 fold higher (22.2
199 RPKM) than those of *AtBOR4* (3.8 RPKM) in roots (Figure 2C, D). We detected two under-
200 studied putative boron transporters (*BOR5* and *BOR7*) that were significantly induced by excess
201 boron. One of these, *BOR5* is the closest homolog of *BOR4* (Takano et al., 2008; Sun et al.,
202 2012; Oh and Dassanayake, 2019). Whereas *BOR5* was induced (~3 fold) by excess boron in *A.*
203 *thaliana* roots (Figure 2C), the *S. parvula* ortholog showed a dramatically higher constitutive
204 expression prior to the stress and represents one of the largest basal expression differences in
205 roots (>2000 fold higher in *S. parvula*) observed among all ortholog pairs between the two
206 species (Figure 2D). *BOR7*, encoding another *BOR4*-like boron transporter (Luo et al., 2019),
207 was also induced in *A. thaliana* roots in response to excess boron, suggesting a putative function
208 to exclude boron under excess boron conditions (Figure 5A). However, *BOR7* was hardly
209 detected at basal levels (lower than 0.1 RPKM) in *A. thaliana* or *S. parvula* roots (Figure 2C).
210 Taken together, our data suggest that, under toxic levels of boron, *A. thaliana* induced the
211 transcript levels for boron transporters implicated in boron exclusion from the roots. On the other
212 hand, in *S. parvula* roots, both *SpBOR4* and *SpBOR5*, although not induced by excess boron,
213 were expressed at a basal level much higher than their orthologs in *A. thaliana*. Therefore, we
214 hypothesized that *BOR5* is functionally active in excluding boron in *S. parvula* roots exposed to
215 excess boron.

216 To further assess the role of SpBOR5 as a key contributor for boron exclusion in *S.*
217 *parvula*, we individually expressed *BOR4* and *BOR5* from each species in a yeast mutant lacking
218 the native boron transporter *ScBOR1* (Figure 2E). This *Δbor* yeast mutant is sensitive to high
219 concentrations of boric acid because of its inability to export excess boron. *SpBOR5* fully
220 rescued the growth of *Δbor* yeast exposed to a toxic level of boron, while *AtBOR4*, *AtBOR5*, or
221 *SpBOR4* failed to complement the *Δbor* mutant growth defects (Figure 2E). This demonstrates
222 that *SpBOR5* functions similar to *ScBOR1* and seems to have a higher boron efflux capacity
223 compared to *AtBOR4*, *AtBOR5*, and *SpBOR4*. These results, together with the strikingly higher
224 basal expression of *SpBOR5* in *S. parvula* roots, suggest that SpBOR5 likely enabled *S. parvula*
225 to exclude excess boron more efficiently than its stress-sensitive relative *A. thaliana*.

226
227 **Transcriptomic responses to boron predict altered cell wall metabolism as a major cellular**
228 **response to enable cell walls to capture excess boron.** We next examined biological processes
229 and functions enriched among the differentially expressed genes (DEGs) in *A. thaliana* roots as it
230 exhibits readily discernible responses when treated with excess boron (Supplemental Data Set 1).
231 From a total of 3,504 boron stress-repressed DEGs, 2,728 could be associated with specific GO
232 functions (Supplemental Data Set 2). Among them, we identified 19 functional clusters using
233 GOMCL (Wang et al., 2020). In short, GOMCL clustered enriched GO terms that had shared
234 genes (>50%) using Markov Clustering and identified non-redundant representative functions
235 within a GO network. The top ten root clusters included over 96% of the GO-annotated DEGs
236 (Figure 3A). This approach revealed that cell wall-related processes account for the largest
237 proportion among boron stress-suppressed DEGs in *A. thaliana* roots. Three of the top ten
238 functional clusters (C2, 7, and 8) were associated with cell wall-related processes, accounting for
239 1,453 DEGs (Figure 3A, red boxes; Supplemental Data Set 2).

240 Next, we expanded our analyses of boron stress-responsive DEGs in functionally
241 enriched clusters to all genes known to be involved in the biosynthesis of major cell wall
242 components (Supplemental Data Set 1). We included both root and shoot tissues to view cell
243 wall biosynthesis-related changes at the whole plant level. Figure 3B summarizes the cell wall
244 biosynthesis pathways, including precursors, intermediates, and the building blocks of cell wall
245 components, together with the genes involved in the process. Cellulose, hemicellulose, and
246 pectin constitute about 90% of cell wall mass (Albersheim et al., 1996; Held et al., 2015).

247 Cellulose is synthesized at the plasma membrane by cellulose synthase (*CesA*) complexes
248 (Schneider et al., 2016; McFarlane et al., 2014), whereas pectins and hemicelluloses are
249 assembled in the Golgi and then exported to the apoplast (Kousar et al., 2012). Hemicelluloses
250 include xyloglucans, xylans, mannans, glucomannans, and mixed-linkage glucans (MLG)
251 (Scheller and Ulvskov, 2010; Pauly et al., 2013), while the predominant pectins are
252 homogalacturonan (HG), rhamnogalacturonan I (RG-I), and rhamnogalacturonan II (RG-II)
253 (Atmodjo et al., 2013).

254 We found that a total of 14 out of 25 *galacturonosyltransferases* (*GAUTs*) and *GAUT-*
255 *like* (*GATL*) genes, which were shown or suggested to be involved in pectin biosynthesis, were
256 DEGs in *A. thaliana* shoots and roots, of which 13 were induced in shoots (Figure 3B,
257 Supplemental Data Set 1). All the *glycosyltransferases* that have been proven or suggested to
258 code for genes (4 *RGXTs* and 2 *SIAs*) involved in assembling the side chains of RG-II on a HG
259 backbone showed a 4-fold or higher increase in *A. thaliana* shoots (Figure 3B, Supplemental
260 Data Set 1). Those *glycosyltransferases* in the roots, however, did not show this induction
261 (Figure 3B). Synergistically, several genes coding for the enzymes (*UXSs* and *UXEs*) producing
262 UDP-arabinopyranose (UDP-*Arap*) and UDP-arabinofuranose (UDP-*Araf*), which are the donors
263 used by glycosyltransferases to incorporate *Arap* and *Araf* into RG-I and RG-II (Bar-Peled and
264 O'Neill, 2011), were also induced in *A. thaliana* shoots, while the majority of other NDP-sugar
265 biosynthesis genes were repressed by excess boron (Figure 3B, left panels). Contrasting to the
266 transcriptomic signal suggesting increased pectin components, the expression of all 10 *CesA*
267 genes coding for cellulose synthases (Carroll and Specht, 2011; McFarlane et al., 2014) together
268 with other genes mostly associated with hemicellulose biosynthesis remained unaffected (Figure
269 3B). The only experimentally verified molecular function of boron in plants is to cross-link RG-
270 II-pectins in the cell wall (Kobayashi et al., 1996; Ishii et al., 1999; O'Neill, 2001; Funakawa and
271 Miwa, 2015). Therefore, a net induction of genes associated with pectin biosynthesis in *A.*
272 *thaliana* shoots suggested a path to potentially bind more boron and trap excess boron in shoot
273 cell walls.

274 The cell wall also contains structural hydroxyproline-rich glycoproteins (HRGPs),
275 notably the extensins (Cannon et al., 2008; Lamport et al., 2011). In *A. thaliana* shoots, excess
276 boron significantly induced genes coding for multiple extensins and glycosyltransferases (GTs)
277 involved in the extensin glycosylation (Velasquez et al., 2011) (Figure 3B and Supplemental

278 Figure 4). It is notable that *A. thaliana* root and shoot expression profiles differed substantially.
279 In roots, virtually all the transcripts potentially coding for extensins that significantly responded
280 to excess boron were suppressed whereas in shoots, transcripts coding for extensins and
281 associated GTs were all induced (Figure 3B). Such a differential regulation of the extensins
282 suggests that the shoot cell wall may be stiffer in *A. thaliana* under excess boron than in the
283 control (Supplemental Figure 4). Stiffening of cell walls has been reported in plants under other
284 abiotic stresses (Tenhaken, 2015). In line with this finding, we also noted the co-repression of
285 many of the genes encoding catalysts of cell wall loosening, including expansins and xyloglucan
286 endotransglucosylase/hydrolases (XTHs) (Cosgrove, 2016) in both shoots and roots (Figure 3B,
287 Supplemental Figure 4). The prominent changes in transcriptional responses related to cell wall
288 biology observed in *A. thaliana* led us to hypothesize that cell walls serves as a sink to store
289 excess boron under boron stress and the associated cell wall modifications were initiated as a
290 transcriptional cascade of several processes including cell wall organization; synthesis and
291 regulation of nucleotide sugar transporters that are linked to cell wall sugars; structural
292 glycoproteins; and cell wall interacting kinases (Figure 3 A-B).

293

294 **Cell wall pectin precursor abundance significantly increased in response to excess boron in**
295 ***A. thaliana* shoots.** Based on the transcriptomic signature that suggested major cell wall
296 modifications, especially related to pectins in *A. thaliana* shoots, we next assessed if such
297 modifications coincided with changes in metabolic pools in boron-stressed shoots. We used GC-
298 MS metabolic profiling to capture the primary metabolite pools from control and treated tissues
299 of *A. thaliana* and *S. parvula*. We detected 39 and 70 annotated metabolites that were
300 differentially accumulated under 5 mM and 10 mM boric acid treatments, respectively
301 (Supplemental Data Set 3). By contrast, the relative abundances of any of these metabolites did
302 not change significantly in *S. parvula* shoots exposed to excess boron (Supplemental Data Set 3).

303 We grouped the functionally annotated organic metabolites that significantly changed in
304 their abundance in response to excess boron into five categories (Supplemental Data Set 3). At
305 least one third of these metabolites were sugars or sugar derivatives, including sugar alcohols,
306 while the remaining pool primarily consisted of amino acids and other amines, fatty acids, and
307 other organic acids (Figure 3C). The organic acids included pyruvic acid, citric acid, and

308 succinic acid. Their abundances are known to change in response to abiotic stresses, which is
309 often associated with changes to overall energy balance during stress (Treves et al., 2020).

310 In line with our transcriptomic data, the relative abundance of many of the free
311 monosaccharides that are components of cell wall polysaccharides, including arabinose,
312 galactose, rhamnose, xylose, and mannose significantly increased upon excess boron in *A.*
313 *thaliana* shoots (Figure 3D and Supplemental Figure 5). Remarkably, the abundance of none of
314 these sugars significantly changed in boron-stressed *S. parvula* (Figure 3D). Arabinose, which is
315 a component of RG-I and RG-II pectic polysaccharides (Bar-Peled and O'Neill, 2011),
316 increased >2.5-fold, together with xylose, the precursor of arabinose (Atmodjo et al., 2013;
317 Seifert, 2018) in response to excess boron in *A. thaliana* shoots (Figure 3D). Rhamnose, which is
318 present in the side chains of RG-II and the backbone of RG-I (Bar-Peled and O'Neill, 2011), also
319 showed a significant increase in response to 10 mM boric acid in *A. thaliana* shoots, together
320 with galactose, another component of RG-I and RG-II. Similarly, the precursors of other cell
321 wall polysaccharides, including mannose, fructose, and glucose increased in response to 10 mM
322 boric acid (Figure 3D). Remarkably, none of these sugars changed significantly in *S. parvula*
323 shoots during any of the boron treatments (Figure 3D). The overall changes in free
324 monosaccharides during excess boron treatment of *A. thaliana* shoots support the view that
325 pectic polysaccharides provide binding sites to trap excess boron in the cell walls.

326 We found that several sugar alcohols in *A. thaliana* shoots, including myo-inositol,
327 cellobiotol, galactinol, erythritol, and glycerol, also increased in response to excess boron (Figure
328 3E). Myo-inositol is a precursor of pectin and hemicellulose (Kanter et al., 2005; Endres and
329 Tenhaken, 2009), and its increase is consistent with our working model that cell wall pectins
330 capture excess boron during boron stress. Cellobiotol and galactinol are also presumed to be
331 involved in cell wall carbohydrate metabolism (Unda et al., 2017). Moreover, some of these
332 sugar alcohols could bind excess boron in a manner similar to sorbitol and mannitol (Brown and
333 Hu, 1998, 1996; Brown et al., 1999). Taken together, our metabolic profiling provide evidence
334 that excess boron led to the increase in sugars and sugar alcohols, many of which are either
335 directly or indirectly related to cell wall polysaccharides in *A. thaliana*.

336

337 **Boron accumulates in the cell walls of *A. thaliana* and *S. parvula*.** We next determined if *A.*
338 *thaliana* and *S. parvula* accumulated boron in their cell walls when grown in excess boron using

339 ICP-MS. In *A. thaliana*, cell wall boron increased in roots and shoots of treated plants compared
340 to the control group (Figure 3F). By contrast, we only detected an increase in boron in *S. parvula*
341 root cell walls (Figure 3F). Cell wall yield remained constant under all tested conditions (Figure
342 3G), even 5 days after the treatments (Supplemental Figure 6). We performed a second series of
343 experiments with four additional biological replicates using an extensive digestion procedure
344 while minimizing possible contaminating boron sources during the experiment (see Methods) to
345 validate boron sequestration in the cell wall during excess boron treatment. These results were
346 consistent with the cell wall boron quantifications we initially performed (Pearson correlation
347 coefficient $r = 0.76$, $P = 0.015$) (Supplemental Figure 7), and confirmed that boron accumulated
348 in the cell walls of *A. thaliana* and *S. parvula*.

349 We next determined if other elements present in plant tissues accumulated in the cell
350 walls as a result of excess boron treatments. None of the 20 elements analyzed differed
351 significantly from control plants in cell walls from *S. parvula* roots and shoots and *A. thaliana*
352 shoots (Supplemental Figure 8). By contrast, almost half of the elements decreased in abundance
353 in root cell walls of excess boron-treated *A. thaliana* (Supplemental Figure 8). This is likely
354 related to the substantial root growth inhibition observed specifically for excess boron-treated *A.*
355 *thaliana*.

356 Our results, when taken together, suggest that cell walls do capture excess boron.
357 Additionally, *A. thaliana* shoot cell walls have a higher capacity to retain boron than their root
358 counterparts (Figure 3F). Since cell wall yield did not change in response to excess boron, the
359 observed changes are likely due to alterations in the internal structures of the cell walls to enable
360 compartmentalization of excess boron. We also observed that the increase in the boron content in
361 *A. thaliana* shoot and root cell walls (>2 fold) was smaller than the increase in boron content in
362 the entire tissue (compare Figures 1H and 3F). This was most notable in *A. thaliana* roots where
363 whole-tissue boron content increased up to 27 fold. A less pronounced, but similar trend was
364 observed for *S. parvula* roots (Figure 3F). Therefore, cell walls may only provide a partial sink
365 for excess boron, and cellular processes involved in cell wall modifications may be limited in the
366 amounts of boron that they can sequester.

367

368 **Altered RNA metabolism in response to excess boron led to an increased mean expression**
369 **of the entire transcriptome in *A. thaliana* roots and shoots.** We next searched for cellular

370 processes that may serve as additional substrates for excess boron or molecular targets that may
371 cause cellular toxicity if bound by excess boron in the cytoplasm. We expected that the genes
372 induced by excess boron may shed light on such processes. Our analysis identified 19 functional
373 clusters comprised of 2,112 of the 2,622 boron stress-induced genes in *A. thaliana* roots, of
374 which the top ten largest clusters represented 99% (2,094) of the total number of genes from all
375 clusters (Supplemental Data Set 2). The most notable cellular process among the induced genes
376 in roots was RNA metabolism described by the largest functional cluster (C1 in Figure 4A).
377 Further, clusters C5, included transcription and translation regulation, and C9, represented by
378 ribosome organization, are also associated with RNA metabolism (Figure 4A, red boxes). This
379 indicates that in *A. thaliana* roots, RNA metabolism-related processes were substantially affected
380 by boron toxicity.

381 To further investigate how RNA metabolism could be altered by excess boron, we
382 examined all genes represented by RNA metabolism (GO:0016070), together with their
383 regulators annotated under specific child GO terms in the *A. thaliana* genome. Interestingly, all
384 RNA metabolism processes, as well as translation and ribosome biogenesis, were enriched in
385 genes differentially responsive to excess boron in our study (Figure 4B). This further confirmed
386 our earlier observation of RNA metabolism being a major target of boron stress, especially in *A.*
387 *thaliana* roots (Figure 4A). There were many more boron stress-induced genes than repressed
388 genes in most of the GO categories especially in *A. thaliana* roots (Figure 4B). For example,
389 RNA processing, RNA modification, ncRNA metabolism, RNA metabolism, RNA secondary
390 structure unwinding, RNA polyadenylation, translation, and ribosome biogenesis all had more
391 genes induced than repressed in each category in roots (Figure 4B, 4C).

392 If RNA metabolism was the most dominant process among the boron stress-induced
393 genes in *A. thaliana*, we hypothesized that the stress effect should be discernible at the entire
394 transcriptome level. Therefore, we tested if the mean expression level per transcript for the entire
395 transcriptome was significantly shifted in the excess boron-treated samples compared to the
396 control, as previously described by Muyle and Gaut (2018). Excess boron stress did lead to an
397 increased mean expression in *A. thaliana* roots and shoots and also in *S. parvula* shoots (Figure
398 4D). The boron stress-adapted *S. parvula*, however, did not show a mean expression change in
399 roots implying its greater capacity to cope with excess boron without a massive change to its
400 entire transcriptome. This may also suggest that the Arabidopsis global transcriptomic response

401 has a significant energetic cost, which could also contribute to the delayed growth during excess
402 boric acid treatments observed (Figure 1).

403

404 ***A. thaliana* roots respond to excess boron by increasing the abundance of multiple amino**
405 **acids, sugars, and nucleic acid-metabolites.** We observed induction of genes especially
406 associated with translation (Figure 4C) and ribosome biogenesis (Figure 4B) in *A. thaliana* roots,
407 which was further supported by the increased average expression level observed for the entire *A.*
408 *thaliana* root transcriptomes (Figure 4D). This led us to test whether changes in RNA
409 metabolism and associated processes observed in the root transcriptomes of *A. thaliana* during
410 excess boron stress affected amino acid usage. Additionally, we suspected that an increased level
411 of translation may also lead to altered metabolic pools of sugars involved in primary energy
412 metabolism especially in *A. thaliana* roots in response to excess boron.

413 The abundance of 32 functionally annotated metabolites changed significantly upon 5 or
414 10 mM boron treatments in *A. thaliana* roots (Supplemental Data Set 3). In contrast, none of
415 these metabolites were affected by either boric acid treatment in *S. parvula* roots (Supplemental
416 Data Set 3). Sugars and amino acids, and their derivatives, constituted the two largest groups of
417 boron stress-responsive metabolites in *A. thaliana* roots (Figure 4E). The relative abundance of 8
418 of the 13 amino acids detected significantly increased in the root tissues in response to the
419 treatments (Figure 4F and Supplemental Data Set 3). This response was more prominent in roots
420 than shoots, where only two out of the 10 amino acids detected changed significantly
421 (Supplemental Data Set 3). The majority of sugars and their derivatives that responded to the
422 treatments in the roots were primarily involved in glycolysis or sugar transport. For example,
423 these included glucopyranose, fructofuranose, glucose 1-phosphate, glucose 6-phosphate,
424 fructose 6-phosphate, sucrose, and raffinose (Supplemental Data Set 3). This may be indicative
425 of the generally higher demand for cellular energy consumption during induced transcription
426 levels especially in *A. thaliana* roots under excess boron stress. Notably, the sugar-metabolite
427 profile in the roots (Supplemental Data Set 3) was quite distinct from the increased abundance of
428 sugars in the shoots that were enriched primarily in cell wall precursors as described earlier
429 (Figure 3D). Ribose, uracil, and adenosine that are related to nucleic acid metabolism also
430 increased in abundance in shoots in response to excess boron, whereas only adenosine from that

431 group increased in the roots (Figure 4G). Adenosine was the metabolite with the highest fold
432 change in shoots and roots among all metabolites detected in our study (Figure 4G).

433

434 **Constitutive expression of *S. parvula* orthologs match the post-stress expression of *A.***
435 ***thaliana* boron stress-responsive orthologs.** To complement our studies focused on boron
436 stress-sensitive *A. thaliana*, we next sought evidence for the types of biological processes that
437 allow *S. parvula* to tolerate toxic amounts of boron. The overall transcriptomic, ionomic, and
438 metabolomic responses elicited in *S. parvula* in response to excess boron were much less
439 pronounced than those for *A. thaliana*. Nevertheless, we were able to observe enriched functions
440 among the differentially expressed genes (Figure 5). Cell wall-modifying enzymes were the only
441 enriched function observed for *S. parvula* roots (Figure 5, Supplemental Data Set 2). Genes
442 encoding protein modifying and mitochondria-localized proteins were also induced in response
443 to the boric acid treatments in *S. parvula* shoots, while genes involved in biotic stress and
444 defense responses and boron uptake were repressed in both roots and shoots (Figure 5,
445 Supplemental Data Set 2).

446 Our comparative -omics framework allows us to gain insight into the *S. parvula* genes
447 and processes that remained unchanged when their orthologs were differentially regulated in *A.*
448 *thaliana* in response to excess boron. To this end, we compared the expression levels of
449 orthologs from the two species under control and treated conditions. We identified ortholog
450 expression for 19,263 pairs in shoots and 19,784 pairs in roots that were used to determine the
451 co-expressed ortholog clusters. This led to 22 shoot and 20 root clusters (Supplemental Data Set
452 4). We further categorized those clusters into four overall expression trends that we have termed
453 as, (a) stress-ready clusters; (b) unique-response clusters; (c) shared-response clusters; and (d)
454 no-response clusters (Figure 6A). In the stress-ready cluster (a), an ortholog from one species
455 responded to the stress to reach a level of expression equivalent to the basal level of the ortholog
456 in the other plants, which itself remain unchanged under the stress. The unique-response clusters
457 (b) represented ortholog pairs where one species showed a response that was unmatched in the
458 other species either at the control or treated levels. Orthologs pairs with a similar response in
459 both species to excess boron stress were categorized into the shared-response cluster (c). Finally,
460 ortholog pairs that did not change their expression to excess boron stress were grouped as “no
461 response” (d).

462 The majority of the ortholog pairs in the two species remained unchanged in response to
463 excess boron (7,797 ortholog pairs from roots and shoots in the no-response group) (Figure 6A).
464 When one ortholog in a pair did respond, the majority (~62%) of those showed only the
465 expression change in the *A. thaliana* ortholog. The ortholog distribution in these categories
466 further highlighted the more restrained transcriptomic responses of *S. parvula* and revealed an
467 interesting but hidden feature of the *S. parvula* genome that we may not have identified without
468 *A. thaliana* as a comparator. We did not identify a single ortholog pair where the *S. parvula*
469 ortholog responded to the stress to reach the basal level of its *A. thaliana* ortholog (i.e. zero
470 representation in the stress-ready group for *A. thaliana*). By contrast, we identified 2,160 *A.*
471 *thaliana* orthologs whose expression changed to match the basal expression observed for the *S.*
472 *parvula* orthologs. Additionally, we only identified 6 *S. parvula* orthologs that could be
473 classified in the unique-response group (Figure 6A). This led us to propose that stress-adapted *S.*
474 *parvula* had a pre-adapted transcriptome with over a thousand orthologs whose basal expression
475 levels (pre-stress expression) match the expression levels achieved in response to the stress
476 (post-stress expression) in stress-sensitive *A. thaliana*. Any differential expression shown by the
477 orthologs in the stress-adapted species prompted by the stress was always echoed by the stress-
478 sensitive species. Thus, these cellular responses may be common among plants responding to
479 excess boron and not restricted by species boundaries.

480 We also identified at least one thousand orthologs in *A. thaliana* roots and shoots that
481 uniquely responded to excess boron. The expression of their *S. parvula* counterparts did not
482 change significantly. We suspect that the majority of the expression changes in *A. thaliana*
483 represent non-specific symptoms caused by interruption to cellular processes in a plant unable to
484 sustain a cellular environment conducive for growth and development rather than a specific
485 response to excess boron.

486 We also searched for enriched functions associated with the stress-ready clusters in *S.*
487 *parvula* to determine what cellular or metabolic processes were enriched at stress-anticipatory
488 levels in the basal transcriptomes. We first looked into the orthologs expressed in the *S. parvula*
489 stress-ready category where *A. thaliana* orthologs were induced in response to excess boron
490 (Figure 6B). These *S. parvula* orthologs were predominantly enriched for RNA metabolic
491 processes (Figure 6C). It should be noted that the same enriched function was also the
492 predominant function among all induced genes in *A. thaliana* roots regardless of their

493 orthologous relationship with *S. parvula* (Figure 4A). We then compared the basal expression
494 levels of all orthologs between *A. thaliana* and *S. parvula* to assess if the basal expression was
495 significantly different between the two species. In both shoots and roots, the *S. parvula*
496 transcriptome showed significant shifts towards overall higher gene expression levels compared
497 to *A. thaliana* (Figure 6D). Taken together, these results suggested that *S. parvula* transcriptomes
498 were pre-adapted for boron stress most notably in the metabolic functions associated with RNA
499 metabolism that was among the most altered processes in the stress-sensitive *A. thaliana* during
500 the excess boron treatments. However, in many of these stress-ready clusters, enriched functions
501 only described a subset of the orthologs, while a significant proportion of orthologs remained
502 functionally uncharacterized (Supplemental Figure 9).

503

504 Discussion

505 Combining our results and previous studies, we propose a model for how excess boron
506 triggers transcriptomic responses that cascade into major cellular and growth responses (Figure
507 7). The stress-sensitive species, *A. thaliana*, in response to boron toxicity: 1) halts active boron
508 uptake; 2) deposits a proportion of excess boron into cell walls; 3) adjusts the expression of
509 genes involved in RNA metabolism; and 4) forms complexes with free boric acid, especially in
510 roots. We demonstrated that boron toxicity induced minimal changes to gene expression,
511 elemental and metabolite profiles, and growth in stress-adapted *S. parvula* when compared to *A.*
512 *thaliana*. Different excess boron tolerance mechanisms are likely present in *S. parvula*. These
513 include, 1) an efficient boron efflux system that minimizes excess boron accumulation in the
514 plant; 2) cell wall absorption of a proportion of excess boron; 3) formation of B-complexes to
515 reduce free boric acid accumulated in the cytoplasm before boron could bind to essential
516 metabolites; and 4) genes associated with cellular processes affected by excess boron in *A.*
517 *thaliana* are constitutively expressed at stress pre-adapted levels.

518

519 ***S. parvula* is equipped with an efficient boron efflux system.** *S. parvula* is an extremophyte
520 that has evolved to grow on boron-rich soils (Nilhan et al., 2008; Oh et al., 2014). As expected, it
521 was less affected by excess boron than the boron stress-sensitive model, *A. thaliana* (Figure 1).
522 This is due in part to the ability of *S. parvula* to maintain relatively low boron levels in its tissues
523 (Figure 1H). This is likely a feature of boron toxicity tolerance since other boron stress-tolerant

524 plants, including *Eutrema salsugineum* (Lamdan et al., 2012) and *Puccinellia distans* (Stiles et
525 al., 2010), also maintain a relatively low level of endogenous boron even when grown under
526 excess boron conditions.

527 At physiological pH, boron primarily exists as uncharged boric acid, which is highly
528 membrane permeable (Reid, 2014). Boric acid readily diffuses into the root cells under adequate
529 or excess boron conditions (Yoshinari and Takano, 2017; Landi et al., 2019; Princi et al., 2016).
530 Several mechanisms have evolved in plants to control boron influx and efflux. For example, *A.*
531 *thaliana* *BOR4* encodes the only boron exporter experimentally shown to function under boron
532 toxicity (Miwa et al., 2014, 2007). Surprisingly, we saw no significant change of expression of
533 this gene in either species in response to excess boron. However, *BOR5*, the closest homolog of
534 *BOR4*, was induced by excess boron in *A. thaliana* roots, and was highly expressed especially in
535 the roots of *S. parvula* control plants (Figure 2C, D). This may be a result of a 15 kb
536 transposition insertion in the upstream region adjacent to the *SpBOR5* transcription start site (Oh
537 et al., 2014). *SpBOR5* and *AtBOR5* exist as single copy genes and are co-linear except for the
538 genomic insertion in *S. parvula* (Oh et al., 2014; Oh and Dassanayake, 2019). We demonstrated
539 that *SpBOR5* is an effective boron exporter (Figure 2D) and propose that it is likely a key
540 contributor to the underlying tolerance of *S. parvula* to excess boron (Figure 7).

541

542 **Excess boron taken into plants is differently compartmentalized in *A. thaliana* and *S.***
543 ***parvula*.** The absorbed excess boron may exist in free or bound forms in plants. We observed
544 that free boric acid levels increased in *A. thaliana* shoots and roots, as well as in *S. parvula*
545 shoots as the external boric acid concentration increased (Figure 1H). Plants may attempt to
546 minimize the deleterious effects of excess boric acid by exporting it to vacuoles. However, we
547 saw no change in the expression of *TIP5;1*, which encodes the only known aquaporin that
548 facilitates boron transport into vacuoles (Pang et al., 2010), in either *A. thaliana* or *S. parvula*
549 (Supplemental Figure 10A). Other boron stress-responsive TIP genes all showed repression
550 instead of induction in treated *A. thaliana* (Supplemental Data Set 1).

551 In a previous study of two barley cultivars that differed in their boron tolerance, the boron
552 stress-tolerant cultivar was reported to have a higher apoplastic boron content than in the
553 sensitive cultivar (Reid and Fitzpatrick, 2009a). We found that the expression levels of *AtBOR5*
554 and *AtBOR7* increased in *A. thaliana* roots in response to excess boric acid (Figure 2C and

555 Supplemental Data Set 1). Therefore, it is possible that a proportion of excess free boric acid is
556 exported into the apoplast, especially in *A. thaliana* roots. Consistent with this notion, previous
557 studies have suggested that apoplastic boric acid constitutes the majority of soluble boron in
558 plants under normal conditions, and even in some species after exposure to excess boron (Matoh,
559 1997). The increase in free boric acid in *A. thaliana* and *S. parvula* is unlikely to be the sole
560 cause of the increased amounts of total boron detected (Figure 1H and I). Rather, some absorbed
561 boron must exist in a bound form especially in *A. thaliana* roots and *S. parvula* shoots. The
562 formation of B-complexes may have contributed to the detoxification of excess boron.
563 Alternatively, such complexes may also accumulate in the cytoplasm as undesirable metabolic
564 end products.

565 Our metabolomic profiles indicated that ribose increased in *A. thaliana* shoots under
566 excess boron (Figure 4G). This monosaccharide together with ribose-containing compounds,
567 including nucleotides, NADH, NAD⁺, and S-adenosylmethionine have the ability to form borate
568 esters in the cytoplasm (Ricardo, 2004; Ralston and Hunt, 2001; Kim et al., 2003, 2004). It is
569 notable that adenosine is among the largest metabolite changes (~65 fold increase) in treated *A.*
570 *thaliana* (Figure 4G). Boron could also form borate esters with sugar alcohols and organic acids
571 containing *cis*-diols (Bolanos et al., 2004). Several sugar alcohols, including galactinol,
572 erythritol, and cellobiotol increased substantially in treated *A. thaliana* shoots (Figure 3E). We
573 also observed that many unidentified compounds changed in *A. thaliana* during boron
574 treatments. Remarkably, none of the identified metabolites changed significantly in *S. parvula* in
575 response to excess boron treatments. This is consistent with our hypothesis of a transcriptome
576 pre-adapted to boron stress in the tolerant *S. parvula* (Supplemental Data Set 3).

577 The lack of substantial changes in the metabolite profiles of *S. parvula* led us to
578 hypothesize two possibilities for how it may minimize the cellular toxicity of excess boron in the
579 cytoplasm. First, generation of borate-containing metabolites may ameliorate toxicity but comes
580 with a high energy cost that would direct *S. parvula* to use more energy efficient alternative
581 paths to store excess boron. Second, if the generation of such B-complexes was harmful but
582 unavoidable when excess boron accumulated in the cytoplasm, *S. parvula* may prevent their
583 accumulation by limiting the amounts of boron in the cytoplasm more efficiently than *A.*
584 *thaliana*. When bound to boron, metabolites in the cytoplasm will be unavailable to critical
585 primary metabolic processes. Thus, cells may attempt to increase the production of these

586 metabolites at a rate that cannot be sustained in boron stress-sensitive species. The response of *A.*
587 *thaliana* to increase many of these metabolites on excess boron are consistent with this view.
588 Alternatively, mechanisms may have developed in *S. parvula* to process excess cytoplasmic
589 boron in a manner that does not preclude ribose or other metabolite pools from functioning in
590 their respective essential roles (Figure 7).

591

592 **Cell wall contributes to partially compartmentalize excess boron.** Several independent
593 studies have provided compelling evidence for the existence of boron-rhamnogalacturonan-II (B-
594 RG-II) complexes in plant cell walls (Kobayashi et al., 1996; Ishii and Matsunaga, 1996; O'Neill
595 et al., 1996). There is also evidence that this complex is required for normal plant growth and
596 development (Fleischer et al., 1999; Ishii et al., 2001; O'Neill, 2001). The carbohydrate-rich
597 plant cell wall is ideally suited to bind boron (Matoh, 1997), but whether cell walls can store
598 excess boron when plants encounter boron toxicity has not been demonstrated. Herein, we
599 provide compelling evidence for this phenomenon. First, we found that while cell wall yield was
600 unaffected, there was an increase in cell wall boron in *A. thaliana* shoots and roots, as well as in
601 *S. parvula* roots, when plants were grown on excess boron (Figure 3F, G). Second, we have
602 demonstrated that boron toxicity altered the expression of many genes involved in cell wall
603 biogenesis or organization as well as pectin biosynthesis (Figure 3A, B). Third, our metabolomic
604 profiling supported the transcriptomic signals related to the changes in the content of cell wall
605 polysaccharide precursors, notably the monosaccharides used to synthesize pectin (Figure 3D).
606 Together these observations strongly support the idea that cell walls contribute, at least partially,
607 to the compartmentation of excess boron in plants (Figure 7).

608 In line with our results, previous studies on *A. thaliana* and boron stress sensitive citrus
609 cultivars showed boron accumulation in the cell sap-free tissue fraction when treated with excess
610 boron (Lamdan et al., 2012)(Martínez-Cuenca et al., 2015). A recent study of the trifoliolate
611 orange (*Poncirus trifoliata*) reported alterations in cell wall structure when plants were treated
612 with excess boron (Riaz et al., 2019; Wu et al., 2019). In contrast to these findings, Dannel et al.
613 (1998) suggested that cell walls did not absorb excess boron during boron toxicity based on
614 studies of boron stress-resistant sunflowers. However, they did not quantify boron accumulation
615 in tissues, and assumed that internal boron levels changed proportionally to the external boron
616 supply; thereby ignoring the possible contribution of active extrusion of excess boron in plants.

617 A subsequent study reexamined boron tolerance in sunflower and concluded that sunflower did
618 exclude excess boron when compared to a sensitive species (Keleş et al., 2011). Several other
619 studies, for example, have noted that barley roots (Hayes and Reid, 2004) and *Eutrema*
620 *salsugineum* shoots (Lamdan et al., 2012) did not store excess boron in the corresponding cell
621 walls. However, these studies did not include both roots and shoots when assessing how excess
622 boron could be partly stored in certain tissues while some of it could be extruded back to the soil.

623 In cell walls, boron can complex with apiose present in RG-II as well as with other sugars
624 containing *cis*-diols (Matoh, 1997). Boron cross-linking of two RG-II molecules occurs rapidly
625 during RG-II synthesis and secretion. Previous studies suggest that the crosslink is formed in the
626 cytoplasm prior to RG-II deposition in cell wall rather than in the cell wall itself (Chormova et
627 al., 2014; Chormova and Fry, 2016). *In vitro* assays have demonstrated that excess boron can
628 reduce the rate of RG-II dimerization (Chormova et al., 2014). Therefore, future studies testing
629 the compositional changes of RG-II and other cell wall sugars during excess boron stress in
630 plants could further identify how plant cell walls may be restructured to allow storage of excess
631 boron.

632

633 **Boron toxicity disturbs RNA metabolism and related processes.** Excess boron resulted in
634 substantial changes in the expression of genes involved in RNA metabolism and related
635 processes, including translation and ribosome biogenesis (Figure 4A). Boron is known to form
636 complexes with ribose (Ricardo, 2004) and ribose-containing compounds *in vitro* (Ralston and
637 Hunt, 2001; Kim et al., 2003, 2004). Thus, one explanation for the extensive changes in RNA
638 metabolism-related processes could be that excess boron affects the availability of ribose and
639 ribose-containing compounds needed for RNA metabolism, and that creates a prominent
640 transcriptional footprint.

641 Uluisik *et al.*, (2011) previously demonstrated that excess boron suppresses protein
642 synthesis and interrupts translation initiation by reducing the proportion of functionally available
643 polysomes in yeast. The authors further showed that excess boron also inhibits aminoacylation of
644 tRNAs *in vitro*. Considering our transcriptomic and metabolomic results, together with the
645 previous publications, it is reasonable to suspect that similar to yeast, excess boron in plants may
646 impact protein synthesis by impairing polysome function. In addition, excess boron may also
647 bind to the ribose moiety at the amino acid attachment site in tRNAs, which could block access

648 to amino acids, thus inhibiting tRNA aminoacylation. In support of this view, our transcriptomic
649 data shows that ribosome biogenesis was enhanced in *A. thaliana* roots and shoots after excess
650 boron treatments (Figure 4B and 7).

651

652 ***S. parvula* transcriptome is pre-adapted to boron toxicity.** Compared to *A. thaliana*, *S.*
653 *parvula* is more tolerant to boron toxicity (Figure 1). Our transcriptomic analyses suggest that *S.*
654 *parvula* is pre-adapted for this stress (Figure 6A). While some of the *S. parvula* orthologs in the
655 “stress-ready” cluster could be readily associated with enriched GO functions (Figure 5), not all
656 orthologs could be represented by GO annotations inferred using experimentally established
657 functions (Supplemental Figure 9). The proteins encoded by many of these genes (>50% in
658 stress-ready clusters) have no known functions described for their *A. thaliana* orthologs. This
659 indicates a severe gap in the functional associations recognized between gene functions relevant
660 to excess boron stress. Our comparative transcriptome analyses indicate that these genes of
661 unknown functions in *A. thaliana* not only respond significantly to excess boron, but also their
662 orthologs in *S. parvula* are expressed at levels comparable to the induced or repressed level in *A.*
663 *thaliana* even in the absence of boron stress. Such stress-preparedness at the transcriptome level
664 is likely a key contributor to the stress response in boron stress-tolerant plants. Indeed, similar
665 transcriptome-level preadaptation to other abiotic stresses have been documented for plants that
666 have evolved in environments where abiotic stresses are a constant feature (Taji et al., 2004;
667 Gong et al., 2005; Becher et al., 2004; Hassan et al., 2016).

668

669 **Why is excess boron toxic to plants?** Our results demonstrated that when plants are grown in
670 the presence of excess boron, some of this boron accumulates in cell walls. However,
671 incorporating boron beyond an undefined threshold may trigger cell wall integrity signaling. We
672 found >55% of genes (at least 300 in shoots and 150 in roots out of 628) coded for receptor-like
673 kinases (RLKs) that responded to excess boron in *A. thaliana* (Supplemental Data Set 1). Many
674 of these genes including *wall-associated kinases (WAKs)*, *Catharanthus roseus RLK1 (CrRLK1)-*
675 *like (CrRLK1L) kinases*, and *leucine-rich repeat (LRR) RLKs* have been suggested to participate
676 in cell wall integrity sensing (Steinwand and Kieber, 2010; Rui and Dinneny, 2019; Vaahtera et
677 al., 2019).

678 We observed that excess boron in *A. thaliana* shoots led to the repression of several
679 *cellulose synthases*, including *CesA2* and *CesA3*, and *CesA* like family members (*CSLD5*)
680 (Supplemental Figure 10B). *CSLD5* is most highly expressed in the shoot meristem of *A.*
681 *thaliana* and is required for initializing cell plate formation (Gu et al., 2016). Boron-dependent
682 repression of *CSLD5* may result in arresting cells in their G2/M transition phase, leading to cell
683 division failures and growth defects. Further, excess boron is reported to decrease the number of
684 mitotic cells and increase the fraction of 4C cells in *A. thaliana* root tips (Sakamoto et al., 2011).
685 Additional studies have reported that inhibition of cellulose biosynthesis leads to the repression
686 of cell cycle genes (Gigli-Bisceglia et al., 2018) and that key core cell cycle regulators are
687 modulated by excess boron (Aquea *et al.* 2012). Our data are consistent with these publications,
688 as we identified cell cycle processes together with exocytosis, which is related to cell-plate
689 formation, as major functional groups among boron stress-repressed genes in *A. thaliana* shoots
690 (Supplemental Figure 11). Therefore, excess boron accumulation in cell walls may not only
691 affect cell wall integrity, but also cell plate construction, which in turn may interrupt cell
692 division. This may explain why the effects of excess boron become apparent in fast-dividing
693 meristems before mature tissue (Choi et al., 2007; Reid et al., 2004; Aquea et al., 2012).

694 Excess boron is not only toxic to plants, but also to yeast and animals (Bakar Salleh et al.,
695 2010; Bakirdere et al., 2014). Therefore, cell wall-mediated boron toxicity alone may not explain
696 the toxic effects of excess boron on these systems, especially animal cells. Excess boron-
697 associated DNA damage has been reported as a consequence of boron toxicity among eukaryotes
698 (Sakamoto et al., 2018). In addition, we showed that transcriptional signals related to RNA
699 metabolism were substantially affected in *A. thaliana*, while *S. parvula* orthologs showed a
700 stress-prepared expression level prior to the stress (Figure 4A, 6A, and 6B). We also observed
701 transcriptome responses pointing to translation as a major target of boron toxicity. Similar results
702 have been reported for yeast (Ulusik et al., 2011). Further, in human cells, excess boron
703 increased the phosphorylation of eIF2 α , which was inferred to lead to reduced protein synthesis
704 (Yamada and Eckhert, 2018; Henderson et al., 2015).

705 In conclusion, we have shown that boron toxicity induces significant physiological and
706 molecular changes in boron stress-sensitive *A. thaliana* compared to stress-adapted *S. parvula*.
707 Excess boron accumulates in the cell walls of both shoots and roots, which may alter the
708 structure and properties of the cell wall and its components. Such changes in the cell wall may

709 affect cell plate formation, which in turn may lead to interruptions in cell division. Our data also
710 suggest that boron toxicity interferes with RNA metabolism-related processes, especially
711 translation, and other metabolic processes that involve ribose-containing metabolites. A model
712 for how excess boron may trigger transcriptomic responses that cascade into major cellular and
713 growth responses is presented in Figure 7. Further studies into cell wall dynamics during excess
714 boron treatments in *A. thaliana*, as well as targeted functional analyses of *A. thaliana* stress-
715 responsive genes that also show “stress-adapted” transcription in *S. parvula* to determine their
716 currently unexplored functions would lead to an extended overview of how plants can survive
717 excess boron stress.

718

719 **Materials and Methods**

720 **Plant material and growth conditions.** *Schrenkiella parvula* (ecotype Lake Tuz) and
721 *Arabidopsis thaliana* (ecotype Col-0) seeds were surface sterilized with Clorox diluted 1:1
722 containing 0.05% Tween-20 and 70% ethanol, followed by 4-5 washes with sterile dH₂O.
723 Sterilized seeds were stratified for 4 days at 4 °C in the dark.

724 Plants for RNAseq, metabolomics, and ionomics experiments, were grown
725 hydroponically in 1/5-strength Hoagland’s solution (Liu et al., 2010; Wang et al., 2018) at 22°C
726 to 24°C in a growth chamber with a 14-h-light/10-h-dark cycle; 100-150 μmol m⁻² s⁻¹ light
727 intensity. 4-week-old plants were transferred to growth media containing fresh 1/5-strength
728 Hoagland’s solution or Hoagland’s solutions containing 5, 10, or 15 mM boric acid. The pH of
729 the media was measured and adjusted to match control solutions in growth media allocated for
730 boric acid treatments. These were kept in the same growth chambers until sample harvest.

731 For seedlings grown on plates, sterilized seeds were germinated on 1/4-strength
732 Murashige and Skoog (MS) agar medium (Murashige and Skoog, 1962). 8-day-old seedlings
733 were transferred to 1/4-strength MS medium with different concentrations of boric acid as
734 indicated in Figure 1 and grown in the same growth chamber as described for 4-week old plants.

735

736 **Measurement of chlorophyll and root length.** Chlorophyll concentrations were determined on
737 a fresh-weight basis. Leaves of 4-week-old *S. parvula* and *A. thaliana* plants were harvested and
738 weighed. Total chlorophyll was extracted with dimethyl sulfoxide solvent (VWR, Radnor, PA),
739 and measured using a SmartSpec™ Plus spectrophotometer (Bio-Rad, Hercules, CA) as

740 described (Richardson et al., 2002). Four biological replicates were used for control and
741 treatments.

742 Root length was measured daily for 7 days for seedlings grown vertically on 1/4-strength
743 MS agar plates. Root length was measured by marking root tip positions daily at the same time
744 for 7 days for both species. On day 7, the plates were scanned and the root lengths quantified
745 using ImageJ (Schneider et al., 2012). Four biological replicates were used with at least 8
746 seedlings per replicate.

747

748 **Elemental analysis.** Shoot and root tissues were harvested at 3 or 24 hours following control
749 (mock) and 5 and 10 mM boric acid treatments. Samples were dried at 37°C for one week in a
750 desiccator to yield between 5 and 60 mg of dry tissue. For quantification of cell wall elements,
751 we prepared cell walls as an alcohol insoluble residue (AIR) as described (Pettolino et al., 2012).
752 Briefly, the harvested tissues were ground to a powder and washed with aq. 80% ethanol,
753 acetone, and methanol. Selected elements (Li, B, Na, Mg, Al, P, S, K, Ca, Fe, Mn, Co, Ni, Cu,
754 Zn, As, Se, Rb, Sr, Mo, and Cd) were quantified using inductively coupled plasma mass
755 spectrometry (ICP-MS) at the United States Department of Agriculture-Agricultural Research
756 Service (USDA-ARS)-Plant Genetics Facility at the Donald Danforth Plant Science Center as
757 described (Baxter *et al.* 2014). Four to five biological replicates were used for each data point.
758 All measurements were normalized to amount per unit weight. One-way ANOVA followed by
759 Tukey's post-hoc tests implemented in R were used to identify significant differences between
760 samples.

761 A second independent ICP-MS analysis with a modified protocol that included a rigorous
762 digestion step was conducted to quantify the boron content in the cell walls and to confirm
763 results obtained in the first ICP-MS quantification. AIR from a second set of four biological
764 replicates were prepared as described below. The AIR was digested with 1 mL ultrapure 70%
765 nitric acid (BDH Aristar® Ultra, VWR, Radnor, PA) in 15 mL Teflon beakers, followed by a
766 serial digestion with 100 µL 70% nitric acid on a 100 °C hot plate overnight. Digestions were
767 carefully dried down to almost complete dryness between each step. Acid washed teflon beakers
768 and trace metal clean tubes were used instead of standard laboratory glassware that contain
769 borosilicate in order to minimize the boron background. A final digestion was performed with
770 100 µL 70% nitric acid and 50 µl 35% H₂O₂ (ACS grade, Ward's Science, Rochester, NY) since

771 undissolved particles remained in solution at the end of the second digestion. The samples were
772 dried on a hot plate as described earlier and the residue dissolved in 5 mL 2% nitric acid. The
773 solution was sonicated for 3-5 mins using an ultrasonic cleaner (FS220, Thermo Fisher
774 Scientific, Waltham, MA). The solution was diluted to 10 mL with 2% nitric acid. Boron was
775 quantified using a Thermo iCap Qc ICP-MS (Thermo Fisher Scientific Inc., Waltham, MA).
776 Internal standard solutions containing ^6Li , ^{45}Sc , ^{89}Y , ^{103}Rh , ^{115}In , ^{193}Ir , ^{209}Bi were added prior to
777 analysis via a Y-split. Quantification was performed using commercially available standards (IV-
778 ICPMS-71A, Inorganic Ventures, Christiansburg, VA). Pearson correlation coefficient between
779 the two independent ICP-MS experiments was computed using the `cor.test` function in R.

780

781 **Identification of orthologs between *S. parvula* and *A. thaliana*.** Genome annotations for *S.*
782 *parvula* version 2.2 (<https://phytozome-next.jgi.doe.gov/>) and *A. thaliana* genome version 10
783 (<https://www.araport.org/>) were used for ortholog identification. When multiple spliced forms
784 existed in *A. thaliana*, the longest version was considered. Orthologous gene pairs as best
785 reciprocal hits between these two species were identified using the CLfinder-OrthNet pipeline
786 with default settings (Oh and Dassanayake, 2019). To account for lineage-specific gene
787 duplications in both species, orthologous gene pairs were searched reciprocally between the two-
788 species using BlastP with an e-value of $1e-5$ and MMseqs2 (Steinegger and Söding, 2017) with
789 an equivalent e-value cutoff. These pairs were further filtered using OrthoFinder (Emms and
790 Kelly, 2015) with granularity -I of 1.6 and were added back to the CLfinder pipeline to extract
791 all possible ortholog pairs between the two species. Among a total of 27,206 *A. thaliana* protein-
792 coding gene models, 22,112 were paired with at least one *S. parvula* homolog. Similarly, 21,673
793 out of 26,847 *S. parvula* gene models were paired with at least one *A. thaliana* ortholog. The two
794 reciprocal searches were merged, and redundant pairs were removed to generate 23,281 *S.*
795 *parvula*-*A. thaliana* orthologous gene pairs.

796

797 **Transcriptome profiling.** Root and shoot tissues were harvested separately for each plant 24
798 hours after boric acid treatment. Total RNA (at least 6 μg) was extracted using the RNeasy Plant
799 Mini kit (Qiagen, Hilden, Germany), with an additional step to remove contaminating DNA.
800 Four biological replicates per condition were generated and three were used for RNA-seq
801 libraries. RNA-seq libraries were prepared with a TruSeq Stranded mRNAseq Sample Prep kit

802 (Illumina, San Diego, CA, USA) at the Roy J. Carver Biotechnology Center, University of
803 Illinois at Urbana-Champaign. Libraries were barcoded and sequenced on three lanes of
804 HiSeq2500 platform (Illumina), generating > 25 million high-quality 100-nucleotide (nt) single-
805 end RNA-seq reads per sample. These reads are deposited in the BioProject PRJNA663969 at
806 the NCBI-SRA database.

807 RNA-seq reads after quality checks using FastQC
808 (<https://www.bioinformatics.babraham.ac.uk/projects/fastqc/>) from each sample were mapped to
809 either *A. thaliana* TAIR10 or *S. parvula* genome v2 using HISAT2 version2.0.1(Kim et al.,
810 2015) with default parameters. A custom Python script was used to count uniquely mapped reads
811 to each gene model found to be expressed. To identify a list of robust differentially expressed
812 genes (DEGs), we used a consensus list from DEGs identified using a parametric method,
813 DESeq2 (Love et al., 2014) and a non-parametric method, NOISeq (Tarazona et al., 2015) with a
814 FDR-adjusted p-value cutoff set to 0.05. Only genes selected by both methods as significantly
815 different were used for down-stream analyses.

816 To compare the expression levels of orthologs between *S. parvula* and *A. thaliana*,
817 expression values of reads per kilobase of transcript per million mapped reads (RPKM) < 1 were
818 removed. The RPKM values of filtered ortholog pairs were converted to log₂-transformed counts
819 and median-normalized. These normalized RPKM values for ortholog pairs across all samples
820 from shoots and roots were subjected to fuzzy k-means clustering (Gasch and Eisen, 2002) to
821 identify co-expressed gene groups. Ortholog pairs in each of the resulting clusters were further
822 filtered based on: (1) the membership of a given ortholog pair was no less than 0.5; (2) the
823 expression changes of each ortholog pair in a given cluster were considered to be statistically
824 significant by both DESeq2 and NOISeq to ensure that the expression pattern of a given pair
825 agreed with that for the cluster; and (3) clusters in which the pattern was consistent between all
826 biological replicates were considered for downstream analyses.

827 BiNGO (Maere et al., 2005) was used to identify enriched networks of Gene Ontology
828 (GO) terms in each species. To reduce the redundancy between enriched GO terms and their
829 associated inference related to DEGs, redundant GO terms with > 50% overlap with similar
830 terms were further clustered using Markov clustering implemented via GOMCL
831 (<https://github.com/Guannan-Wang/GOMCL>) (Wang et al., 2020). Custom Python scripts were
832 used to extract all direct child terms of a given GO term or all genes annotated with the given

833 GO term. GO terms with zero assigned genes from *A. thaliana* were removed from the analysis.
834 Kyoto Encyclopedia of Genes and Genomes (KEGG) (Kanehisa et al., 2016) was used to map
835 genes to specific metabolic pathways.

836

837 **RT-qPCR.** Plants were grown and treated with excess boric acid and harvested as described for
838 RNA-seq experiments. Total RNA (0.5 µg) was used in a 20 µL reverse transcription (RT)
839 reaction for first-strand cDNA synthesis with SuperScript™ III Reverse Transcriptase according
840 to the manufacturer's instructions (Invitrogen, Carlsbad, CA). The reverse transcription products
841 were diluted to 200 µL, and 2 µL was used in a 20 µL qPCR reaction using SYBR™ Select
842 Master Mix (Applied Biosystems, Foster City, CA) in a ViiA 7 Real-Time PCR System (Applied
843 Biosystems, Foster City, CA).

844 Our transcriptomic profiles showed that the commonly used reference genes, *ACT2*,
845 *CYTC-1*, *CYTC-2*, *EF1α*, *UBQ10*, and *GAPDH*, all had expression levels that varied between
846 treatments, plants, and tissue types, which made them unsuitable as reference genes in RT-qPCR.
847 Therefore, we searched for the most uniformly expressed and conserved genes in both plants and
848 selected At5g46630 (ADAPTOR PROTEIN-2 MU-ADAPTIN) and At4g26410 (RGS1-HXK1
849 INTERACTING PROTEIN 1) and their *S. parvula* orthologs as internal reference genes,
850 following the best practice recommendations from previous studies (Czechowski et al., 2005;
851 Wang et al., 2014). RT-qPCR primer sequences are listed in Supplemental Data Set 5.

852

853 **Metabolomics analyses.** Shoot and root samples were harvested at 24 hours after control, 5, and
854 10 mM boric acid treatments and freeze dried (FreeZone 2.5 Plus, Labconco Corp., Kansas City,
855 MS). Untargeted profiling of polar metabolites, including boric acid, using gas chromatography-
856 mass spectrometry (GC-MS) was performed at the Metabolomics Center at University of
857 Missouri, Columbia. To facilitate the detection of trace metabolites, 20 mg of roots or 50 mg of
858 shoots from pools of 7-12 plants were used per biological replicate per condition. The dry tissues
859 were suspended in 1.0 ml of aq. 80% methanol and 20 µl of HPLC grade water containing 1
860 µg/ml ribitol. The suspensions were vortexed for 20 seconds, and sonicated for 15 min. The
861 suspensions were shaken for 2 hours at 140 rpm in an orbital shaker and centrifuged for 30
862 minutes at 15000 g. Equal amounts of the supernatant were transferred to autosampler vials. The
863 solutions were concentrated to dryness using a gaseous nitrogen stream. The dried extracts were

864 methoximated with 25 μ l of 15 mg/mL methoxyamine hydrochloride in pyridine, and
865 trimethylsilylated with 25 μ L N-methyl-N-(trimethyl-silyl)trifluoroacetamide (MSTFA) and 1%
866 chlorotrimethylsilane (TMCS). The derivatized extracts were analyzed for non-targeted
867 metabolic profiling using an Agilent 6890 GC coupled to a 5973N MSD mass spectrometer with
868 a scan range from m/z 50 to 650 (Agilent Technologies, Inc., Santa Clara, CA). 1 μ l of sample
869 was injected into the GC column with a split ratio of 1:1 for polar GC-MS analysis. Separation
870 was achieved using a 60 m DB-5MS column (J&W Scientific, 0.25 mm ID, 0.25 μ m film
871 thickness) with a temperature program of 80 $^{\circ}$ C for 2 min, then ramped at 5 $^{\circ}$ C /min to 315 $^{\circ}$ C
872 and held at 315 $^{\circ}$ C for 12 min, and a constant flow of helium gas (1.0 ml/min). A standard alkane
873 mix was used for GC-MS quality control and retention index calculations. The raw data were
874 first deconvoluted using AMDIS software
875 (<http://chemdata.nist.gov/dokuwiki/doku.php?id=chemdata:amdis>) and annotated through mass
876 spectral and retention index matching to an in-house spectra library. The unidentified compounds
877 were searched and identified using spectral matching to a commercial NIST17 mass spectral
878 library. The raw abundance/intensity for each identified compound was normalized with the
879 internal standard, ribitol (peak area of each metabolite/peak area of internal standard \times 1,000).
880 Different molecular features were manually curated to the most relevant molecular feature for
881 each identified metabolite. A minimum of three biological replicates were used for each
882 condition for each tissue. Significant differences between samples were determined by Student's
883 t tests followed by FDR correction for multiple testing (Benjamini and Hochberg, 1995) in
884 MetaboAnalystR (Chong et al., 2019).

885
886 **Yeast complementation assay.** Yeast Δbor mutant strains were in the *MAT α ADE2 his3 Δ 1*
887 *leu Δ D0 lys2 Δ 0 TRP1 ura3 Δ 0 bor1D::KanMX* background. The entire coding regions of
888 *AtBOR4*, *AtBOR5*, *SpBOR4*, *SpBOR5* were cloned from *A. thaliana* and *S. parvula* cDNA,
889 respectively, and were separately introduced into the pDD506 plasmid (Wang and Donze, 2016),
890 driven by the ADH1 promoter. The Δbor mutant was transformed with the recombinant pDD506
891 plasmids or the empty pDD506 plasmid as a negative control. The transformants were selected
892 on SD medium-His. Boron toxicity tolerance assays were performed as described in Nozawa *et*
893 *al.* (2006). Briefly, yeast cells were grown in SD medium to OD₆₀₀=1, collected, and spotted

894 onto solid SD or SD containing 80 mM boric acid with different titers. The plates were
895 photographed after incubation for 10 days at 30 °C.

896

897 **Supplemental Data**

898 **Supplemental Figure 1.** Ionic profiles in response to boric acid treatments. Significant
899 differences of each treatment compared to control were based on one-way ANOVA followed by
900 Tukey's post-hoc tests ($p < 0.05$).

901 **Supplemental Figure 2.** Differential expression visualized using MA-plots from shoot (left
902 panel) and root (right panel) of *A. thaliana* (upper panel) and *S. parvula* (lower panel). Red dots
903 represent up-regulated DEGs and blue dots indicate down-regulated DEGs.

904 **Supplemental Figure 3.** Assessment of qPCR and RNA-seq expression data agreement for
905 selected differentially expressed genes.

906 **Supplemental Figure 4.** Summary of cell wall modifications in *A. thaliana* in response to boric
907 acid treatment. Genes are represented by in colored blocks, grouped into families and pathways,
908 with up- and down-regulation marked by red and blue, respectively.

909 **Supplemental Figure 5.** Relative abundances of sugars in *A. thaliana* shoots that are not directly
910 associated with cell wall polysaccharides. The relative abundance is given compared to the
911 internal standard, ribitol. Values shown are mean \pm SD ($n = 3, 4$ or 5). Asterisks represent
912 significant differences of each treatment compared to control according to Student's t test ($p <$
913 0.05).

914 **Supplemental Figure 6.** Cell wall content in *A. thaliana* and *S. parvula* treated with excess
915 boron for 5 days. Values shown are mean \pm SD ($n = 3$ or 4).

916 **Supplemental Figure 7.** Conformance of boron content quantified using two independent
917 experiments. Fold changes were calculated comparing the treatment to the control for each tissue
918 from each species. Pearson's r and p -values are indicated.

919 **Supplemental Figure 8.** Ionic profiles in the cell wall extracts in response to boric acid
920 treatments at 24 hours. Significant differences of each treatment compared to control for each
921 element were based on one-way ANOVA followed by Tukey's post-hoc tests ($p < 0.05$).

922 **Supplemental Figure 9.** Number of members and their annotation availability in selected stress-
923 ready clusters. RC: root cluster; SC: shoot cluster.

924 **Supplemental Figure 10.** Expression levels of *TIP5;1* and *CSLD5* from *A. thaliana* and *S.*
925 *parvula* in control and 5 mM boric acid treatment. Asterisks represent significant differences in
926 expression compared to control (at FDR-adjusted $p < 0.05$) determined by both DESeq2 and
927 NOISeq.

928 **Supplemental Figure 11.** Functional clusters enriched among genes that were induced (A) and
929 repressed (B) in *A. thaliana* shoots. Top 10 largest clusters are differently colored and labelled
930 with the representative functional terms. Each node represents a GO term; node size represents
931 genes in the test set assigned to that functional term; GO terms sharing more than 50% of genes
932 are connected with edges; and shade of each node represents the p -value assigned by the
933 enrichment test (FDR-adjusted $p < 0.05$) with darker shades indicating smaller p -values.

934 **Supplemental Data Set 1.** The list of DEGs identified from DESeq2 and NOIseq, and list of
935 genes used for pathway analysis.

936 **Supplemental Data Set 2.** Functional clusters enriched in boron stress-responsive genes in *A.*
937 *thaliana* and *S. parvula*.

938 **Supplemental Data Set 3.** List of differentially accumulated metabolites and their functional
939 categories.

940 **Supplemental Data Set 4.** Co-expression clusters of orthologs between *A. thaliana* and *S.*
941 *parvula*.

942 **Supplemental Data Set 5.** Primer sequences used for qPCR.

943

944 **Acknowledgements**

945 This work was supported by the National Science Foundation awards MCB-1616827 and NSF-
946 IOS-EDGE-1923589 to MD, DHO, and APS. MD also acknowledges the support from the Next-
947 Generation BioGreen21 Program of Republic of Korea (PJ01317301). GW was supported by an
948 Economic Development Assistantship award from Louisiana State University. MAO
949 acknowledges the Division of Chemical Sciences, Geosciences, and Biosciences, Office of Basic
950 Energy Sciences of the United States Department of Energy through Grant DE-SC0008472 for
951 funding studies of plant cell walls. DMC acknowledges NSF through award MCB-1818312. The
952 authors thank Dr. David Donze (Biological Sciences, LSU) for providing necessary yeast strains
953 and advice on the yeast assays and Katherine Winchester (high school student, St. Joseph's
954 Academy, Baton Rouge) for her assistance with root phenotyping. The authors also acknowledge

955 the LSU High Performance Computing services for providing computational resources needed
956 for data analyses.

957

958 **Author contributions**

959 GW and MD developed the experimental design; GW prepared plant samples, conducted data
960 analyses, and performed RT-qPCR; SFD performed yeast assays; ADH and GW designed and
961 conducted the ICP-MS assays. GW, DHO, DMC, MAO, APS, and MD contributed to data
962 interpretation. GW and MD wrote the article with input from all co-authors who revised and
963 approved the final manuscript.

964

965 **Competing interests**

966 The authors declare no competing interests.

967

968 **Additional information**

969 Correspondence and requests for materials should be addressed to MD.

970

971 **References:**

972 **Albersheim, P., Darvill, A.G., O'Neill, M.A., Schols, H.A., and Voragen, A.G.J.** (1996). An
973 hypothesis: The same six polysaccharides are components of the primary cell walls of all
974 higher plants. *Pectins and Pectinases* **14**: 47–55.

975 **Aquea, F., Federici, F., Moscoso, C., Vega, A., Jullian, P., Haseloff, J., and Arce-Johnson,**
976 **P.** (2012). A molecular framework for the inhibition of Arabidopsis root growth in response
977 to boron toxicity. *Plant. Cell Environ.* **35**: 719–34.

978 **Atmodjo, M.A., Hao, Z., and Mohnen, D.** (2013). Evolving Views of Pectin Biosynthesis.
979 *Annu. Rev. Plant Biol.* **64**: 747–779.

980 **Ayers, R.S. and Westcot, D.W.** (1985). *Water Quality for Agriculture* (Vol. 29).

981 **Bakar Salleh, A., Swi See, A., Abu Bakar, F., Azah Yusof, N., Sahib Abdulmir, A., and**
982 **Yook Heng, L.** (2010). Risk and Health Effect of Boric Acid. *Am. J. Appl. Sci.* **7**: 620–627.

983 **Bakirdere, S., Orenay, S., and Korkmaz, M.** (2014). Effect of Boron on Human Health. *Open*
984 *Miner. Process. J.*

985 **Bar-Peled, M. and O'Neill, M.A.** (2011). Plant Nucleotide Sugar Formation, Interconversion,

- 986 and Salvage by Sugar Recycling*. *Annu. Rev. Plant Biol.* **62**: 127–155.
- 987 **Baxter, I.R., Ziegler, G., Lahner, B., Mickelbart, M. V., Foley, R., Danku, J., Armstrong,**
988 **P., Salt, D.E., and Hoekenga, O.A.** (2014). Single-kernel ionic profiles are highly
989 heritable indicators of genetic and environmental influences on elemental accumulation in
990 maize grain (*Zea mays*). *PLoS One*.
- 991 **Becher, M., Talke, I.N., Krall, L., and Krämer, U.** (2004). Cross-species microarray transcript
992 profiling reveals high constitutive expression of metal homeostasis genes in shoots of the
993 zinc hyperaccumulator *Arabidopsis halleri*. *Plant J.*
- 994 **Benjamini, Y. and Hochberg, Y.** (1995). Controlling the False Discovery Rate: A Practical and
995 Powerful Approach to Multiple Testing. *J. R. Stat. Soc. Ser. B.*
- 996 **Bolanos, L., Lukaszewski, K., Bonilla, I., and Blevins, D.** (2004). Why boron? *Plant Physiol*
997 *Biochem* **42**: 907–912.
- 998 **Brenchley, W.E.** (1914). On the Action of Certain Compounds of Zinc, Arsenic, and Boron on
999 the Growth of Plants. *Ann. Bot.* **os-28**: 283–301.
- 1000 **Broadley, M., Brown, P., Cakmak, I., Rengel, Z., and Zhao, F.** (2012). Function of Nutrients.
1001 In *Marschner's Mineral Nutrition of Higher Plants* (Elsevier), pp. 191–248.
- 1002 **Brown, P.H., Bellaloui, N., Wimmer, M.A., Bassil, E.S., Ruiz, J., Hu, H., Pfeffer, H.,**
1003 **Dannel, F., and Romheld, V.** (2002). Boron in plant biology. *Plant Biol* **4**: 205–223.
- 1004 **Brown, P.H. and Hu, H.** (1998). Phloem boron mobility in diverse plant species. *Bot. Acta* **111**:
1005 331–335.
- 1006 **Brown, P.H. and Hu, H.** (1996). Phloem mobility of boron is species dependent: Evidence for
1007 phloem mobility in sorbitol-rich species. *Ann. Bot.* **77**: 497–506.
- 1008 **Brown, P.H., Hu, H., and Roberts, W.G.** (1999). Occurrence of sugar alcohols determines
1009 boron toxicity symptoms of ornamental species. *J. Am. Soc. Hortic. Sci.* **124**: 347–352.
- 1010 **Camacho-cristóbal, J.J., Rexach, J., and González-Fontes, A.** (2008). Boron in plants:
1011 Deficiency and toxicity. *J. Integr. Plant Biol.* **50**: 1247–1255.
- 1012 **Cannon, M.C., Terneus, K., Hall, Q., Tan, L., Wang, Y., Wegenhart, B.L., Chen, L.,**
1013 **Lampert, D.T.A., Chen, Y., and Kieliszewski, M.J.** (2008). Self-assembly of the plant
1014 cell wall requires an extensin scaffold. *Proc. Natl. Acad. Sci.* **105**: 2226–2231.
- 1015 **Carroll, A. and Specht, C.D.** (2011). Understanding Plant Cellulose Synthases through a
1016 Comprehensive Investigation of the Cellulose Synthase Family Sequences. *Front. Plant Sci.*

- 1017 **2: 5.**
- 1018 **Choi, E.Y., Kolesik, P., McNeill, A., Collins, H., Zhang, Q., Huynh, B.L., Graham, R., and**
1019 **Stangoulis, J.** (2007). The mechanism of boron tolerance for maintenance of root growth in
1020 barley (*Hordeum vulgare* L.). *Plant, Cell Environ.* **30**: 984–993.
- 1021 **Chong, J., Yamamoto, M., and Xia, J.** (2019). MetaboAnalystR 2.0: From raw spectra to
1022 biological insights. *Metabolites*.
- 1023 **Chormova, D. and Fry, S.C.** (2016). Boron bridging of rhamnogalacturonan-II is promoted in
1024 vitro by cationic chaperones, including polyhistidine and wall glycoproteins. *New Phytol.*
1025 **209**: 241–251.
- 1026 **Chormova, D., Messenger, D.J., and Fry, S.C.** (2014). Boron bridging of rhamnogalacturonan-
1027 II, monitored by gel electrophoresis, occurs during polysaccharide synthesis and secretion
1028 but not post-secretion. *Plant J.* **77**: 534–546.
- 1029 **Cook, F.C. and Wilson, J.B.** (1918). Boron: Its effect on crops and its distribution in plants and
1030 soil in different parts of the United States. *J. Agric. Res* **13**: 451–470.
- 1031 **Copeland, E.B. and Kahlenberg, L.** (1899). The influence of the presence of pure metals upon
1032 plants (Wisconsin Academy of Sciences, Arts and Letters).
- 1033 **Cosgrove, D.J.** (2016). Catalysts of plant cell wall loosening. *F1000Research* **5**: 119.
- 1034 **Czechowski, T., Stitt, M., Altmann, T., Udvardi, M.K., and Scheible, W.-R.** (2005).
1035 Genome-wide identification and testing of superior reference genes for transcript
1036 normalization in *Arabidopsis*. *Plant Physiol.* **139**: 5–17.
- 1037 **Dannel, F., Pfeffer, H., and Römheld, V.** (1998). Compartmentation of boron in roots and
1038 leaves of sunflower as affected by boron supply. *J Plant Physiol* **153**: 615–622.
- 1039 **Dassanayake, M., Oh, D.-H.H., Haas, J.S., Hernandez, A., Hong, H., Ali, S., Yun, D.-J.J.,**
1040 **Bressan, R.A., Zhu, J.-K.K., Bohnert, H.J., and Cheeseman, J.M.** (2011). The genome
1041 of the extremophile crucifer *Thellungiella parvula*. *Nat. Genet.* **43**: 913–918.
- 1042 **Diehn, T.A., Bienert, M.D., Pommerrenig, B., Liu, Z., Spitzer, C., Bernhardt, N., Fuge, J.,**
1043 **Bieber, A., Richet, N., Chaumont, F., and Bienert, G.P.** (2019). Boron demanding tissues
1044 of *Brassica napus* express specific sets of functional Nodulin26-like Intrinsic Proteins and
1045 BOR 1 transporters. *Plant J.*: 1–15.
- 1046 **Eaton, F.M.** (1935). Boron in Soils and Irrigation Waters and Its Effect on Plants, With
1047 Particular Reference to the San Joaquin Valley of California. U. S. Dept. Agr. Tech. Bull.

- 1048 **448.**
- 1049 **Eaton, F.M.** (1944). Deficiency, toxicity and accumulation of boron in plants. *J. Agric. Res.* **69**:
1050 237–279.
- 1051 **Eaton, S. V.** (1940). EFFECTS OF BORON DEFICIENCY AND EXCESS ON PLANTS. *Plant*
1052 *Physiol.* **15**: 95–107.
- 1053 **Emms, D.M. and Kelly, S.** (2015). OrthoFinder: solving fundamental biases in whole genome
1054 comparisons dramatically improves orthogroup inference accuracy. *Genome Biol.* **16**: 1–14.
- 1055 **Endres, S. and Tenhaken, R.** (2009). Myoinositol oxygenase controls the level of myoinositol
1056 in Arabidopsis, but does not increase ascorbic acid. *Plant Physiol.*
- 1057 **Fleischer, a, O’Neill, M., and Ehwald, R.** (1999). The Pore Size of Non-Graminaceous Plant
1058 Cell Walls Is Rapidly Decreased by Borate Ester Cross-Linking of the Pectic
1059 Polysaccharide Rhamnogalacturonan II. *Plant Physiol.* **121**: 829–838.
- 1060 **Funakawa, H. and Miwa, K.** (2015). Synthesis of borate cross-linked rhamnogalacturonan II.
1061 *Front. Plant Sci.* **6**: 1–8.
- 1062 **Gasch, A.P. and Eisen, M.B.** (2002). Exploring the conditional coregulation of yeast gene
1063 expression through fuzzy k-means clustering. *Genome Biol.* **3**: RESEARCH0059.
- 1064 **Gigli-Bisceglia, N., Engelsdorf, T., Strnad, M., Vaahtera, L., Khan, G.A., Yamoune, A.,**
1065 **Alipanah, L., Novák, O., Persson, S., Hejatko, J., and Hamann, T.** (2018). Cell wall
1066 integrity modulates Arabidopsis thaliana cell cycle gene expression in a cytokinin- and
1067 nitrate reductase-dependent manner. *Development* **145**: dev166678.
- 1068 **Goldberg, S.** (1997). Reactions of boron with soils. *Plant Soil* **193**: 35–48.
- 1069 **Gong, Q., Li, P., Ma, S., Indu Rupassara, S., and Bohnert, H.J.** (2005). Salinity stress
1070 adaptation competence in the extremophile *Thellungiella halophila* in comparison with its
1071 relative Arabidopsis thaliana. *Plant J.* **44**: 826–839.
- 1072 **Grieve, C.M., Grattan, S.R., and Maas, E. V.** (2011). Plant Salt Tolerance. In *Agricultural*
1073 *Salinity Assessment and Management* (American Society of Civil Engineers: Reston, VA),
1074 pp. 405–459.
- 1075 **Gu, F., Bringmann, M., Combs, J.R., Yang, J., Bergmann, D.C., and Nielsen, E.** (2016).
1076 Arabidopsis CSLD5 functions in cell plate formation in a cell cycle-dependent manner.
1077 *Plant Cell.*
- 1078 **Haas, A.R.C.** (1929). Toxic Effect of Boron on Fruit Trees. *Bot. Gaz.* **88**: 113–131.

- 1079 **Hassan, M. Al, Pacurar, A., López-Gresa, M.P., Donat-Torres, M.P., Llinares, J. V.,**
1080 **Boscaiu, M., and Vicente, O.** (2016). Effects of salt stress on three ecologically distinct
1081 plantago species. *PLoS One* **11**: 1–21.
- 1082 **Hayes, J. and Reid, R.** (2004). Boron tolerance in barley is mediated by efflux of B from the
1083 roots. *Plant Physiol.* **136**: 3376–3382.
- 1084 **Held, M.A., Jiang, N., Basu, D., Showalter, A.M., and Faik, A.** (2015). Plant Cell Wall
1085 Polysaccharides: Structure and Biosynthesis. In *Polysaccharides: bioactivity and*
1086 *biotechnology* (Springer International Publishing: Cham), pp. 3–54.
- 1087 **Helvacı, C., Mordogan, H., Çolak, M., and Gündogan, I.** (2004). Presence and Distribution of
1088 Lithium in Borate Deposits and Some Recent Lake Waters of West-Central Turkey. *Int.*
1089 *Geol. Rev.* **46**: 177–190.
- 1090 **Henderson, K.A., Kobylewski, S.E., Yamada, K.E., and Eckhert, C.D.** (2015). Boric acid
1091 induces cytoplasmic stress granule formation, eIF2 α phosphorylation, and ATF4 in prostate
1092 DU-145 cells. *BioMetals* **28**: 133–141.
- 1093 **Hu, H. and Brown, P.H.** (1997). Absorption of boron by plant roots. *Plant Soil* **193**: 49–58.
- 1094 **Ishii, T. and Matsunaga, T.** (1996). Isolation and characterization of a boron-
1095 rhamnogalacturonan-II complex from cell walls of sugar beet pulp. *Carbohydr. Res.* **284**: 1–
1096 9.
- 1097 **Ishii, T., Matsunaga, T., and Hayashi, N.** (2001). Formation of rhamnogalacturonan II-borate
1098 dimer in pectin determines cell wall thickness of pumpkin tissue. *Plant Physiol.* **126**: 1698–
1099 1705.
- 1100 **Ishii, T., Matsunaga, T., Pellerin, P., O’Neill, M.A., Darvill, A., and Albersheim, P.** (1999).
1101 The Plant Cell Wall Polysaccharide Rhamnogalacturonan II Self-assembles into a
1102 Covalently Cross-linked Dimer. *J. Biol. Chem.* **274**: 13098–13104.
- 1103 **Julkowska, M.M.** (2018). Adjusting Boron Transport by Two-Step Tuning of Levels of the
1104 Efflux Transporter BOR1. *Plant Physiol.* **177**: 439–440.
- 1105 **Kanehisa, M., Sato, Y., Kawashima, M., Furumichi, M., and Tanabe, M.** (2016). KEGG as a
1106 reference resource for gene and protein annotation. *Nucleic Acids Res.* **44**: D457–D462.
- 1107 **Kanter, U., Usadel, B., Guerineau, F., Li, Y., Pauly, M., and Tenhaken, R.** (2005). The
1108 inositol oxygenase gene family of Arabidopsis is involved in the biosynthesis of nucleotide
1109 sugar precursors for cell-wall matrix polysaccharides. *Planta*.

- 1110 **Kazachkova, Y., Eshel, G., Pantha, P., Cheeseman, J.M., Dassanayake, M., and Barak, S.**
1111 (2018). Halophytism: What Have We Learnt From Arabidopsis thaliana Relative Model
1112 Systems? *Plant Physiol.* **178**: 972–988.
- 1113 **Keleş, Y., Ergün, N., and Öncel, I.** (2011). Antioxidant enzyme activity affected by high boron
1114 concentration in sunflower and tomato seedlings. *Commun. Soil Sci. Plant Anal.* **42**: 173–
1115 183.
- 1116 **Kim, D., Langmead, B., and Salzberg, S.L.** (2015). HISAT: a fast spliced aligner with low
1117 memory requirements. *Nat. Methods* **12**: 357–360.
- 1118 **Kim, D.H., Faull, K.F., Norris, A.J., and Eckhert, C.D.** (2004). Borate-nucleotide complex
1119 formation depends on charge and phosphorylation state. *J. Mass Spectrom.* **39**: 743–751.
- 1120 **Kim, D.H., Marbois, B.N., Faull, K.F., and Eckhert, C.D.** (2003). Esterification of borate with
1121 NAD⁺ and NADH as studied by electrospray ionization mass spectrometry and ¹¹B NMR
1122 spectroscopy. *J. Mass Spectrom.* **38**: 632–640.
- 1123 **Kobayashi, M., Matoh, T., and Azuma, J.** (1996). Two Chains of Rhamnogalacturonan II Are
1124 Cross-Linked by Borate-Diol Ester Bonds in Higher Plant Cell Walls. *Plant Physiol.* **110**:
1125 1017–1020.
- 1126 **Kousar, S., Vicro-Gibouin, M., Bernard, S., Follet-Gueye, M.-L., Lerouxel, O., Chevalier,
1127 L., and Driouich, A.** (2012). Golgi-Mediated Synthesis and Secretion of Matrix
1128 Polysaccharides of the Primary Cell Wall of Higher Plants. *Front. Plant Sci.* **3**: 1–15.
- 1129 **Lamdan, N.L., Attia, Z., Moran, N., and Moshelion, M.** (2012). The Arabidopsis-related
1130 halophyte *Thellungiella halophila*: boron tolerance via boron complexation with
1131 metabolites? *Plant. Cell Environ.* **35**: 735–46.
- 1132 **Lamport, D.T.A., Kieliszewski, M.J., Chen, Y., and Cannon, M.C.** (2011). Role of the
1133 Extensin Superfamily in Primary Cell Wall Architecture. *Plant Physiol.* **156**: 11–19.
- 1134 **Landi, M., Margaritopoulou, T., Papadakis, I.E., and Araniti, F.** (2019). Boron toxicity in
1135 higher plants: an update. *Planta*.
- 1136 **Liu, W.-J., Wood, B.A., Raab, A., McGrath, S.P., Zhao, F.-J., and Feldmann, J.** (2010).
1137 Complexation of Arsenite with Phytochelatins Reduces Arsenite Efflux and Translocation
1138 from Roots to Shoots in Arabidopsis. *Plant Physiol.* **152**: 2211–2221.
- 1139 **Lovatt, C.J. and Bates, L.M.** (1984). Early effects of excess boron on photosynthesis and
1140 growth of *Cucurbita pepo*. *J. Exp. Bot.* **35**: 297–305.

- 1141 **Love, M.I., Huber, W., and Anders, S.** (2014). Moderated estimation of fold change and
1142 dispersion for RNA-seq data with DESeq2. *Genome Biol.* **15**: 550.
- 1143 **Luo, J., Liang, Z., Wu, M., and Mei, L.** (2019). Genome-wide identification of BOR genes in
1144 poplar and their roles in response to various environmental stimuli. *Environ. Exp. Bot.* **164**:
1145 101–113.
- 1146 **Maere, S., Heymans, K., and Kuiper, M.** (2005). BiNGO: a Cytoscape plugin to assess
1147 overrepresentation of Gene Ontology categories in Biological Networks. *Bioinformatics* **21**:
1148 3448–3449.
- 1149 **Martínez-Cuenca, M.-R., Martínez-Alcántara, B., Quiñones, A., Ruiz, M., Iglesias, D.J.,**
1150 **Primo-Millo, E., and Forner-Giner, M.Á.** (2015). Physiological and Molecular Responses
1151 to Excess Boron in *Citrus macrophylla* W. *PLoS One* **10**: e0134372.
- 1152 **Matoh, T.** (1997). Boron in plant cell walls. *Plant Soil* **193**: 59–70.
- 1153 **McFarlane, H.E., Döring, A., and Persson, S.** (2014). The Cell Biology of Cellulose Synthesis.
1154 *Annu. Rev. Plant Biol.* **65**: 69–94.
- 1155 **Miwa, K., Aibara, I., and Fujiwara, T.** (2014). *Arabidopsis thaliana* BOR4 is upregulated
1156 under high boron conditions and confers tolerance to high boron. *Soil Sci. Plant Nutr.* **60**:
1157 349–355.
- 1158 **Miwa, K., Takano, J., Omori, H., Seki, M., Shinozaki, K., and Fujiwara, T.** (2007). Plants
1159 tolerant of high boron levels. *Science* (80-.). **318**: 1417.
- 1160 **Murashige, T. and Skoog, F.** (1962). A Revised Medium for Rapid Growth and Bio Assays
1161 with Tobacco Tissue Cultures. *Physiol. Plant.*
- 1162 **Muyle, A. and Gaut, B.S.** (2018). Loss of gene body methylation in *Eutrema salsugineum* is
1163 associated with reduced gene expression. *Mol. Biol. Evol.*: 1–4.
- 1164 **Nable, R.O., Bañuelos, G.S., and Paull, J.G.** (1997). Boron toxicity. *Plant Soil* **193**: 181–198.
- 1165 **Nilhan, T.G., Emre, Y.A., and Osman, K.** (2008). Soil Determinants for Distribution of
1166 *Halocnemum strobilaceum* Bieb. (Chenopodiaceae) Around Lake Tuz, Turkey. *Pakistan J.*
1167 *Biol. Sci.* **11**: 565–570.
- 1168 **Nozawa, A., Miwa, K., Kobayashi, M., and Fujiwara, T.** (2006). Isolation of *Arabidopsis*
1169 *thaliana* cDNAs That Confer Yeast Boric Acid Tolerance. *Biosci. Biotechnol. Biochem.* **70**:
1170 1724–1730.
- 1171 **O’Neill, M.A.** (2001). Requirement of Borate Cross-Linking of Cell Wall Rhamnogalacturonan

- 1172 II for Arabidopsis Growth. *Science* (80-.). **294**: 846–849.
- 1173 **O’Neill, M.A., Warrenfeltz, D., Kates, K., Pellerin, P., Doco, T., Darvill, A.G., and**
1174 **Albersheim, P.** (1996). Rhamnogalacturonan-II, a pectic polysaccharide in the walls of
1175 growing plant cell, forms a dimer that is covalently cross-linked by a borate ester. In vitro
1176 conditions for the formation and hydrolysis of the dimer. *J. Biol. Chem.* **271**: 22923–22930.
- 1177 **Oh, D.-H., Hong, H., Lee, S.Y., Yun, D.-J., Bohnert, H.J., and Dassanayake, M.** (2014).
1178 Genome structures and transcriptomes signify niche adaptation for the multiple-ion-tolerant
1179 extremophyte *Schrenkiella parvula*. *Plant Physiol.* **164**: 2123–38.
- 1180 **Oh, D. and Dassanayake, M.** (2019). Landscape of gene transposition–duplication within the
1181 Brassicaceae family. *DNA Res.* **26**: 21–36.
- 1182 **Pang, Y., Li, L., Ren, F., Lu, P., Wei, P., Cai, J., Xin, L., Zhang, J., Chen, J., and Wang, X.**
1183 (2010). Overexpression of the tonoplast aquaporin *AtTIP5;1* conferred tolerance to boron
1184 toxicity in *Arabidopsis*. *J. Genet. Genomics* **37**: 389–397.
- 1185 **Pauly, M., Gille, S., Liu, L., Mansoori, N., de Souza, A., Schultink, A., and Xiong, G.** (2013).
1186 Hemicellulose biosynthesis. *Planta* **238**: 627–642.
- 1187 **Pettolino, F.A., Walsh, C., Fincher, G.B., and Bacic, A.** (2012). Determining the
1188 polysaccharide composition of plant cell walls. *Nat. Protoc.* **7**: 1590–1607.
- 1189 **Princi, M.P., Lupini, A., Araniti, F., Longo, C., Mauceri, A., Sunseri, F., and Abenavoli,**
1190 **M.R.** (2016). Boron Toxicity and Tolerance in Plants. In *Plant Metal Interaction* (Elsevier),
1191 pp. 115–147.
- 1192 **Ralston, N.V.C. and Hunt, C.D.** (2001). Diadenosine phosphates and S-adenosylmethionine:
1193 Novel boron binding biomolecules detected by capillary electrophoresis. *Biochim. Biophys.*
1194 *Acta - Gen. Subj.* **1527**: 20–30.
- 1195 **Reid, R.** (2010). Can we really increase yields by making crop plants tolerant to boron toxicity?
1196 *Plant Sci.* **178**: 9–11.
- 1197 **Reid, R.** (2014). Understanding the boron transport network in plants. *Plant Soil.*
- 1198 **Reid, R.** (2007). Update on Boron Toxicity and Tolerance in Plants. In *Advances in Plant and*
1199 *Animal Boron Nutrition*, pp. 83–90.
- 1200 **Reid, R. and Fitzpatrick, K.** (2009a). Influence of Leaf Tolerance Mechanisms and Rain on
1201 Boron Toxicity in Barley and Wheat. *Plant Physiol.* **151**: 413–420.
- 1202 **Reid, R.J.** (2013). Boron Toxicity and Tolerance in Crop Plants. In *Crop Improvement Under*

- 1203 Adverse Conditions (Springer New York: New York, NY), pp. 333–346.
- 1204 **Reid, R.J. and Fitzpatrick, K.L.** (2009b). Redistribution of boron in leaves reduces boron
1205 toxicity. *Plant Signal. Behav.* **4**: 1091–1093.
- 1206 **Reid, R.J., Hayes, J.E., Post, A., Stangoulis, J.C.R., and Graham, R.D.** (2004). A critical
1207 analysis of the causes of boron toxicity in plants. *Plant. Cell Environ.* **27**: 1405–1414.
- 1208 **Riaz, M., Yan, L., Wu, X., Hussain, S., Aziz, O., El-Desouki, Z., and Jiang, C.** (2019).
1209 Excess boron inhibited the trifoliolate orange growth by inducing oxidative stress, alterations
1210 in cell wall structure, and accumulation of free boron. *Plant Physiol. Biochem.* **141**: 105–
1211 113.
- 1212 **Ricardo, A.** (2004). Borate Minerals Stabilize Ribose. *Science* (80-.). **303**: 196–196.
- 1213 **Richardson, A.D., Duigan, S.P., and Berlyn, G.P.** (2002). An evaluation of noninvasive
1214 methods to estimate foliar chlorophyll content. *New Phytol.* **153**: 185–194.
- 1215 **Rui, Y. and Dinneny, J.R.** (2019). A wall with integrity: surveillance and maintenance of the
1216 plant cell wall under stress. *New Phytol.*
- 1217 **Ruiz, J.M., Rivero, R.M., and Romero, L.** (2003). Preliminary studies on the involvement of
1218 biosynthesis of cysteine and glutathione concentration in the resistance to B toxicity in
1219 sunflower plants. *Plant Sci.* **165**: 811–817.
- 1220 **Sakamoto, T., Inui, Y.T., Uraguchi, S., Yoshizumi, T., Matsunaga, S., Mastui, M., Umeda,**
1221 **M., Fukui, K., and Fujiwara, T.** (2011). Condensin II alleviates DNA damage and is
1222 essential for tolerance of boron overload stress in Arabidopsis. *Plant Cell* **23**: 3533–46.
- 1223 **Sakamoto, T., Tsujimoto-Inui, Y., Sotta, N., Hirakawa, T., Matsunaga, T.M., Fukao, Y.,**
1224 **Matsunaga, S., and Fujiwara, T.** (2018). Proteasomal degradation of BRAHMA promotes
1225 Boron tolerance in Arabidopsis. *Nat. Commun.* **9**: 5285.
- 1226 **Scheller, H.V. and Ulvskov, P.** (2010). Hemicelluloses. *Annu. Rev. Plant Biol.* **61**: 263–289.
- 1227 **Schneider, C.A., Rasband, W.S., and Eliceiri, K.W.** (2012). NIH Image to ImageJ: 25 years of
1228 image analysis. *Nat. Methods* **9**: 671–675.
- 1229 **Schneider, R., Hanak, T., Persson, S., and Voigt, C.A.** (2016). Cellulose and callose synthesis
1230 and organization in focus, what’s new? *Curr. Opin. Plant Biol.* **34**: 9–16.
- 1231 **Seifert, G.J.** (2018). Mad moves of the building blocks - Nucleotide sugars find unexpected
1232 paths into cell walls. *J. Exp. Bot.* **69**: 905–907.
- 1233 **Steinegger, M. and Söding, J.** (2017). MMseqs2 enables sensitive protein sequence searching

- 1234 for the analysis of massive data sets. *Nat. Biotechnol.* **35**: 2–4.
- 1235 **Steinwand, B.J. and Kieber, J.J.** (2010). The role of receptor-like kinases in regulating cell
1236 wall function. *Plant Physiol.* **153**: 479–484.
- 1237 **Stiles, A.R., Bautista, D., Atalay, E., Babaoğlu, M., and Terry, N.** (2010). Mechanisms of
1238 boron tolerance and accumulation in plants: A physiological comparison of the extremely
1239 boron-tolerant plant species, *puccinellia distans*, with the moderately boron-tolerant
1240 *gypsophila arrostil*. *Environ. Sci. Technol.* **44**: 7089–7095.
- 1241 **Sun, J., Shi, L., Zhang, C., and Xu, F.** (2012). Cloning and characterization of boron
1242 transporters in *Brassica napus*. *Mol. Biol. Rep.* **39**: 1963–1973.
- 1243 **Taji, T., Seki, M., Satou, M., Sakurai, T., Kobayashi, M., Ishiyama, K., Narusaka, Y.,**
1244 **Narusaka, M., Zhu, J.-K., and Shinozaki, K.** (2004). Comparative Genomics in Salt
1245 Tolerance between *Arabidopsis* and *Arabidopsis*-Related Halophyte Salt Cress Using
1246 *Arabidopsis* Microarray. *Plant Physiol.* **135**: 1697–1709.
- 1247 **Takano, J., Miwa, K., and Fujiwara, T.** (2008). Boron transport mechanisms: collaboration of
1248 channels and transporters. *Trends Plant Sci* **13**: 451–457.
- 1249 **Takano, J., Noguchi, K., Yasumori, M., Kobayashi, M., Gajdos, Z., Miwa, K., Hayashi, H.,**
1250 **Yoneyama, T., and Fujiwara, T.** (2002). *Arabidopsis* boron transporter for xylem loading.
1251 *Nature* **420**: 337–340.
- 1252 **Takano, J., Wada, M., Ludewig, U., Schaaf, G., von Wirén, N., Fujiwara, T., Takano, J.,**
1253 **Wada, M., Ludewig, U., Schaaf, G., von Wirén, N., and Fujiwara, T.** (2006). The
1254 *Arabidopsis* Major Intrinsic Protein NIP5 ; 1 Is Essential for Efficient Boron Uptake and
1255 Plant Development under Boron Limitation. *Plant Cell* **18**: 1498–1509.
- 1256 **Tarazona, S., Furió-Tarí, P., Turrà, D., Di Pietro, A., Nueda, M.J., Ferrer, A., and Conesa,**
1257 **A.** (2015). Data quality aware analysis of differential expression in RNA-seq with NOISeq
1258 R/Bioc package. *Nucleic Acids Res.* **43**.
- 1259 **Tenhaken, R.** (2015). Cell wall remodeling under abiotic stress. *Front. Plant Sci.* **5**: 1–9.
- 1260 **Treves, H. et al.** (2020). Multi-omics reveals mechanisms of total resistance to extreme
1261 illumination of a desert alga. *Nat. Plants* **6**: 1031–1043.
- 1262 **Ulusik, I., Kaya, A., Fomenko, D.E., Karakaya, H.C., Carlson, B.A., Gladyshev, V.N., and**
1263 **Koc, A.** (2011). Boron stress activates the general amino acid control mechanism and
1264 inhibits protein synthesis. *PLoS One* **6**.

- 1265 **Unda, F., Kim, H., Hefer, C., Ralph, J., and Mansfield, S.D.** (2017). Altering carbon
1266 allocation in hybrid poplar (*Populus alba* × *grandidentata*) impacts cell wall growth and
1267 development. *Plant Biotechnol. J.*
- 1268 **Vaahtera, L., Schulz, J., Hamann, T., and Sciences, N.** (2019). Cell wall integrity
1269 maintenance during plant development and interaction with the environment. *Nat. Plants* **5**:
1270 924–932.
- 1271 **Velasquez, S.M. et al.** (2011). O-Glycosylated Cell Wall Proteins Are Essential in Root Hair
1272 Growth. *Science* (80-.). **332**: 1401–1403.
- 1273 **Wang, C., Na, G., Bermejo, E.S., Chen, Y., Banks, J.A., Salt, D.E., and Zhao, F.-J.** (2018).
1274 Dissecting the components controlling root-to-shoot arsenic translocation in *Arabidopsis*
1275 *thaliana*. *New Phytol.* **217**: 206–218.
- 1276 **Wang, G., Oh, D.H., and Dassanayake, M.** (2020). GOMCL: A toolkit to cluster, evaluate, and
1277 extract non-redundant associations of Gene Ontology-based functions. *BMC*
1278 *Bioinformatics.*
- 1279 **Wang, H., Wang, J., Jiang, J., Chen, S., Guan, Z., Liao, Y., and Chen, F.** (2014). Reference
1280 genes for normalizing transcription in diploid and tetraploid *arabidopsis*. *Sci. Rep.*
- 1281 **Wang, Q. and Donze, D.** (2016). Transcription factor Reb1 is required for proper transcriptional
1282 start site usage at the divergently transcribed TFC6-ESC2 locus in *Saccharomyces*
1283 *cerevisiae*. *Gene* **594**: 108–116.
- 1284 **Warington, K.** (1937). Boron in Agriculture. *Nature* **140**: 1016–1016.
- 1285 **Woods, W.G.** (1996). Review of possible boron speciation relating to its essentiality. *J. Trace*
1286 *Elem. Exp. Med.* **9**: 153–163.
- 1287 **Wu, X., Lu, X., Riaz, M., Yan, L., and Jiang, C.** (2019). Boron toxicity induced specific
1288 changes of cell ultrastructure and architecture of components in leaf center and tip of
1289 trifoliolate orange [*Poncirus trifoliata* (L.) Raf.]. *J. Environ. Manage.* **246**: 426–433.
- 1290 **Yamada, K.E. and Eckhert, C.D.** (2018). Boric Acid Activation of eIF2 α and Nrf2 Is PERK
1291 Dependent: a Mechanism that Explains How Boron Prevents DNA Damage and Enhances
1292 Antioxidant Status. *Biol. Trace Elem. Res.*
- 1293 **Yoshinari, A. and Takano, J.** (2017). Insights into the mechanisms underlying boron
1294 homeostasis in plants. *Front. Plant Sci.* **8**: 1–8.
- 1295 **Zhu, J.K.** (2015). The Next Top Models. *Cell* **163**: 18–20.

1296

1297

1298 **Figure Legends**

1299 **Figure 1.** *A. thaliana* and *S. parvula* respond to boric acid treatments differently. (A)
1300 Hydroponically grown 33-day-old *A. thaliana* and *S. parvula* with different concentrations of
1301 boric acid. Boric acid treatments started at 4-week-old plants. Scale bars = 5 cm. (B) Growth
1302 phenotype of 2-week-old *A. thaliana* and *S. parvula* on plates with boric acid. Plants were
1303 germinated and grown on 1/4 MS medium, transferred to 1/4 MS medium supplemented with
1304 boric acid one week after the germination. (C) Dry biomass and (D) total chlorophyll content of
1305 hydroponically grown *A. thaliana* and *S. parvula*. (E) Root growth, (F) lateral root density, and
1306 (G) average lateral root length of plate-grown *A. thaliana* and *S. parvula* seedlings. (H) Boron
1307 and (I) free boric acid accumulation in shoots and roots in *A. thaliana* and *S. parvula*. In panels
1308 C-I, all values are mean \pm SD (n=3~5, except for E where n=14~15). Asterisks represent
1309 significant differences (p<0.05) compared to control determined by either one-way ANOVA
1310 followed by Tukey's post-hoc tests (C-H) or Student's t-test (I).

1311
1312 **Figure 2.** Transcriptional responses of *A. thaliana* and *S. parvula* to excess boron. (A) Principal
1313 component analysis (PCA) differentiates the transcriptomes of control and treated samples from
1314 shoot and root tissues of *A. thaliana* (left) and *S. parvula* (right). (B) PCA of *A. thaliana* and *S.*
1315 *parvula* transcriptomes within shoot (left) and root (right). (C) Expression levels of BOR1,
1316 NIP5;1, BOR4, BOR5, BOR7 in control and 5 mM boric acid treatment. Asterisks represent
1317 significant differences in expression compared to control (at FDR-adjusted p<0.05) determined
1318 by both DESeq2 and NOISeq. (D) Comparison of the basal expression levels of ortholog pairs in
1319 roots between *A. thaliana* and *S. parvula*. Ortholog pairs that encode boron transporters and
1320 channels are marked in red. Gray diagonal dashed line marks identical basal level expression
1321 between the two species while ortholog pairs above the red dashed line show >2000-times higher
1322 basal expression in *S. parvula* than in *A. thaliana*. (E). Growth of yeast *Δbor* mutants
1323 transformed with either *ScBOR1*, *AtBOR4*, *AtBOR5*, *SpBOR4*, or *SpBOR5* on medium containing
1324 0 and 80 mM boric acid. Negative control was transformed with the empty vector.

1325
1326 **Figure 3.** Cell wall metabolism is altered under boron toxicity in *A. thaliana*. (A) Functional
1327 clusters enriched among boron stress-repressed genes in *A. thaliana* roots. Clusters associated
1328 with cell wall metabolism are marked by red-dashed boxes. Clusters are differently colored and

1329 labelled with the representative functional term. Each node represents a GO term; node size
1330 represents genes in the test set assigned to that functional term; GO terms sharing more than 50%
1331 of genes are connected with edges; and shade of each node represents the p -value assigned by the
1332 enrichment test (FDR-adjusted $p < 0.05$) with darker shades indicating smaller p -values. (B)
1333 Changes in gene expression associated with biosynthesis of cell wall components in response to
1334 boric acid treatment in *A. thaliana* shoots and roots. Genes are represented by square blocks,
1335 grouped by families or pathways, with up- and down-regulation marked by red and blue,
1336 respectively. UDP, uridine diphosphate; UDP-Glc, UDP-glucose; UDP-Gal, UDP-galactose;
1337 UDP-GlcA, UDP-glucuronic acid; UDP-GalA, UDP-galacturonic acid; UDP-Xyl, UDP-xylose;
1338 UDP-Ara, UDP-arabinose; UDP-Araf, UDP-arabinofuranose; UDP-Rha, UDP-rhamnose; UDP-
1339 Api, UDP-apiose; GDP-Man, GDP-mannose; GDP-Fuc, GDP-fucose; GDP-Gal, GDP-galactose;
1340 GAE, UDP-D-glucuronic acid 4-epimerase; UXS, UDP-D-xylose synthase; UXE, UDP-D-
1341 xylose 4-epimerase; RGP, reversibly glycosylated protein; AXS, UDP-D-apiose/UDP-D-xylose
1342 synthase (also known as UAXS); MIOX, inositol oxygenase; UGD, UDP-D-glucose
1343 dehydrogenase; UGP/USP, UDP-glucose pyrophosphorylase/UDP-sugar pyrophosphorylase;
1344 RHM/UER, rhamnose synthase gene/ nucleotide-rhamnose epimerase-reductase; UGE, UDP-D-
1345 glucose 4-epimerase; GMP, GDP-D-mannose pyrophosphorylase; GMD/GER, GDP-D-
1346 mannose-4,6-dehydratase/GDP-4-keto-6-deoxy-D-mannose-3,5-epimerase-4-reductase; GME,
1347 GDP-D-mannose 3,5-epimerase; EXTs, extensins; EXT GTs, extensin glycosyltransferases;
1348 EXPs, expansins; XTHs, xyloglucan endotransglucosylase/hydrolases; RGXT,
1349 rhamnogalacturonan xylosyltransferase. (C) Major organic metabolic groups that changed their
1350 abundance in response to excess boron stress in *A. thaliana* shoots. For each category, the
1351 number and proportion of metabolites that changed in abundance compared to the total identified
1352 are shown. (D-E) Monosaccharide precursors of cell wall polysaccharides (D) and sugar alcohols
1353 (E) that changed in abundance in shoots of *A. thaliana* and *S. parvula* 24 hours after boric acid
1354 treatments. The relative abundance is given compared to the internal standard, ribitol. (F) Boron
1355 contents in cell walls extracted from shoots and roots of *A. thaliana* and *S. parvula* under
1356 different treatments for 24 hours. (G) Cell wall yield of shoots and roots in *A. thaliana* and *S.*
1357 *parvula* exposed to different treatments for 24 hours. Cell wall yield was calculated as the
1358 percentage of plant biomass on a dry weight basis. In panels D-G, all values are mean \pm SD

1359 (n=3~5). Asterisks represent significant differences ($p < 0.05$) compared to control determined by
1360 Student's t-test.

1361

1362 **Figure 4.** RNA metabolism related processes are affected in response to excess boron in *A.*
1363 *thaliana*. (A) Enriched functional clusters among boron stress-induced genes in *A. thaliana* roots
1364 with notable associations for RNA metabolism marked by red-dashed boxes. The network
1365 visualization is similar to Figure 3A. (B-C) Number of boron stress responsive genes from *A.*
1366 *thaliana* in functional categories associated with RNA metabolism (B) and translation
1367 (GO:0006412). (C). Red and blue indicate up- and down-regulation, respectively. (D) Global
1368 transcriptome expression distributions in *A. thaliana* and *S. parvula*. Density distributions of
1369 expression in $\log(\text{RPKM}+1)$ for entire transcriptomes were compared to identify transcriptome-
1370 wide global changes. *p*-values were estimated using Wilcoxon signed-rank test. (E) Major
1371 organic metabolic groups that changed their abundance in response to excess boron stress in *A.*
1372 *thaliana* roots. For each category, the number and proportion of metabolites that changed in
1373 abundance compared to the total identified are shown. (F) Amino acid and (G) nucleic acid-
1374 metabolite abundance changes in response to excess boron stress in shoot and root. The relative
1375 abundance is given compared to the internal standard, ribitol. Values shown are mean \pm SD (n =
1376 3, 4 or 5). Asterisks represent significant differences of each treatment compared to control
1377 according to Student's t test ($p < 0.05$).

1378

1379 **Figure 5.** Functional clusters enriched among differentially expressed genes in *S. parvula* in
1380 response to excess boron. The network visualization was constructed the same way described for
1381 Figure 3A. Numbers assigned for each cluster represent total number of genes from all
1382 subclusters/total number of boron stress-responsive genes in the category.

1383

1384 **Figure 6.** Genes associated with excess boron responses are constitutively expressed in *S.*
1385 *parvula*. (A) Summary of co-expression trends in ortholog pairs between *A. thaliana* and *S.*
1386 *parvula* in response to excess boron. The red lines indicate the trend in expression levels of the
1387 ortholog pairs in each species under control and treatment conditions, compared to *A. thaliana*
1388 control (dashed line). Ctrl, Control; + B, boric acid treatment; S, Shoot; R, Root. (B) A major co-
1389 expression cluster in the “stress-ready” category in (A) that illustrates stress preparedness of the

1390 *S. parvula* orthologs in roots (center line, median; box, interquartile range (IQR); notch, $1.58 \times$
1391 IQR / \sqrt{n}); whiskers, $1.5 \times IQR$). (C) Functional clusters enriched among the ortholog pairs
1392 from the example cluster given in (B). The clusters are differently colored and labelled with the
1393 representative functions. Node size represents genes in the test set which are annotated to that
1394 functional term; edges represent the number of shared genes between functional terms; each
1395 cluster is coded with a different color; and shade of each node represents p -value assigned by the
1396 enrichment test. Lighter to darker shades indicate larger to smaller p -values, respectively. (D) *S.*
1397 *parvula* shows a higher basal level expression than *A. thaliana*. p -values were estimated using
1398 Wilcoxon signed-rank test.

1399

1400 **Figure 7.** A proposed model for boron toxicity in plants.

1401

1402

1403

1404

1405

1406

1407

1408

1409

1410

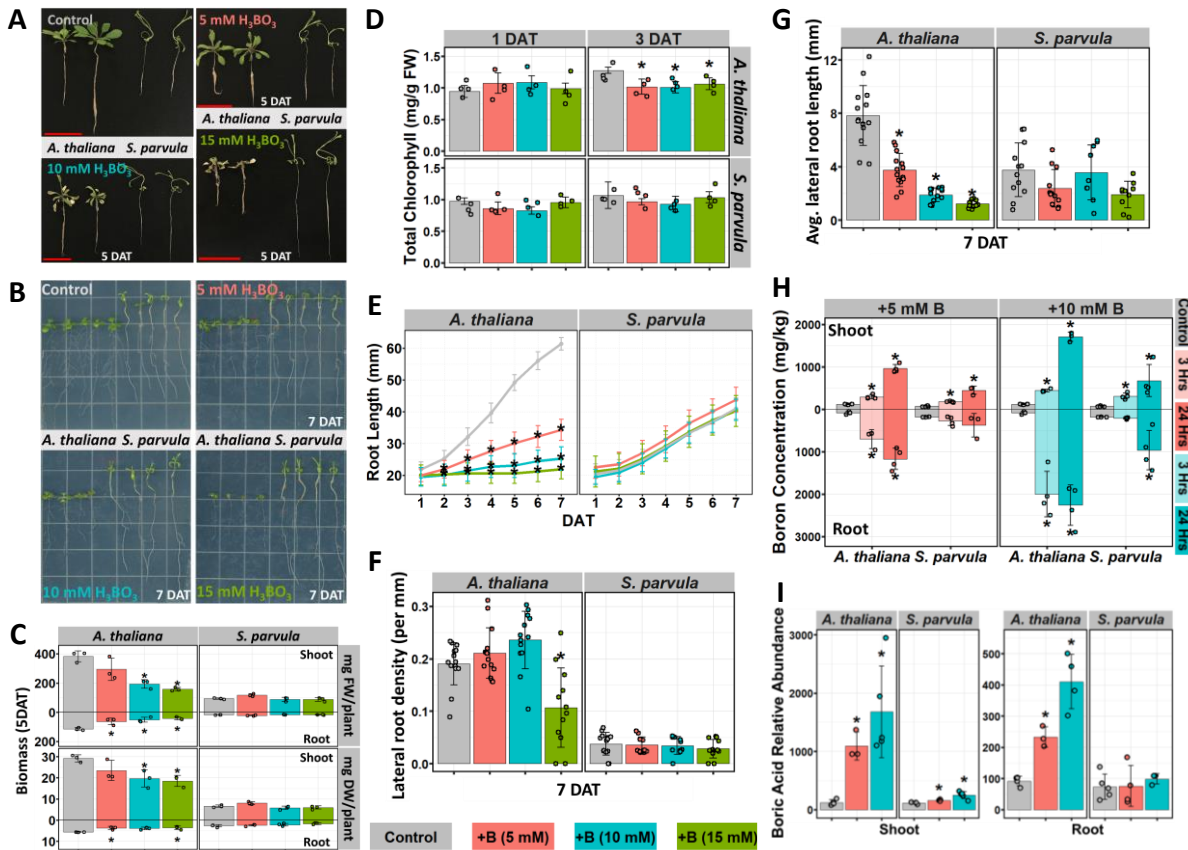


Figure 1. *A. thaliana* and *S. parvula* respond to boric acid treatments differently. (A) Hydroponically grown 33-day-old *A. thaliana* and *S. parvula* with different concentrations of boric acid. Boric acid treatments started at 4-week-old plants. Scale bars = 5 cm. (B) Growth phenotype of 2-week-old *A. thaliana* and *S. parvula* on plates with boric acid. Plants were germinated and grown on 1/4 MS medium, transferred to 1/4 MS medium supplemented with boric acid one week after the germination. (C) Dry biomass and (D) total chlorophyll content of hydroponically grown *A. thaliana* and *S. parvula*. (E) Root growth, (F) lateral root density, and (G) average lateral root length of plate-grown *A. thaliana* and *S. parvula* seedlings. (H) Boron and (I) free boric acid accumulation in shoots and roots in *A. thaliana* and *S. parvula*. In panels C-I, all values are mean \pm SD (n=3~5, except for E where n=14~15). Asterisks represent significant differences (p<0.05) compared to control determined by either one-way ANOVA followed by Tukey's post-hoc tests (C-H) or Student's t-test (I).

1411

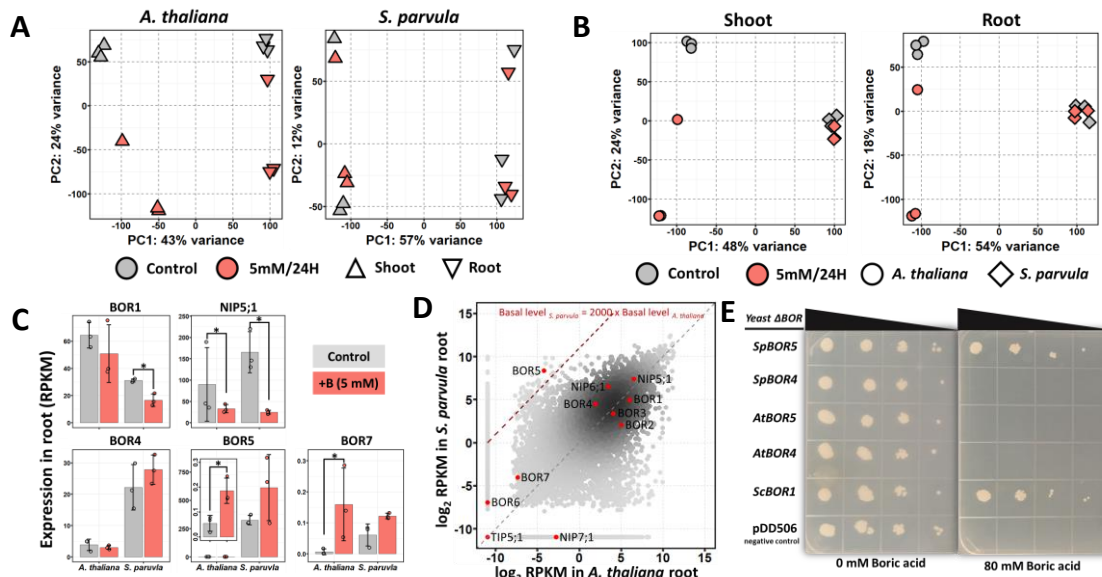


Figure 2. Transcriptional responses of *A. thaliana* and *S. parvula* to excess boron. (A) Principal component analysis (PCA) differentiates the transcriptomes of control and treated samples from shoot and root tissues of *A. thaliana* (left) and *S. parvula* (right). (B) PCA of *A. thaliana* and *S. parvula* transcriptomes within shoot (left) and root (right). (C) Expression levels of BOR1, NIP5;1, BOR4, BOR5, BOR7 in control and 5 mM boric acid treatment. Asterisks represent significant differences in expression compared to control (at FDR-adjusted $p < 0.05$) determined by both DESeq2 and NOISeq. (D) Comparison of the basal expression levels of ortholog pairs in roots between *A. thaliana* and *S. parvula*. Ortholog pairs that encode boron transporters and channels are marked in red. Gray diagonal dashed line marks identical basal level expression between the two species while ortholog pairs above the red dashed line show $>2000\times$ higher basal expression in *S. parvula* than in *A. thaliana*. (E). Growth of yeast ΔBOR mutants transformed with either *ScBOR1*, *AtBOR4*, *AtBOR5*, *SpBOR4*, or *SpBOR5* on medium containing 0 and 80 mM boric acid. Negative control was transformed with the empty vector.

1412

1413

1414

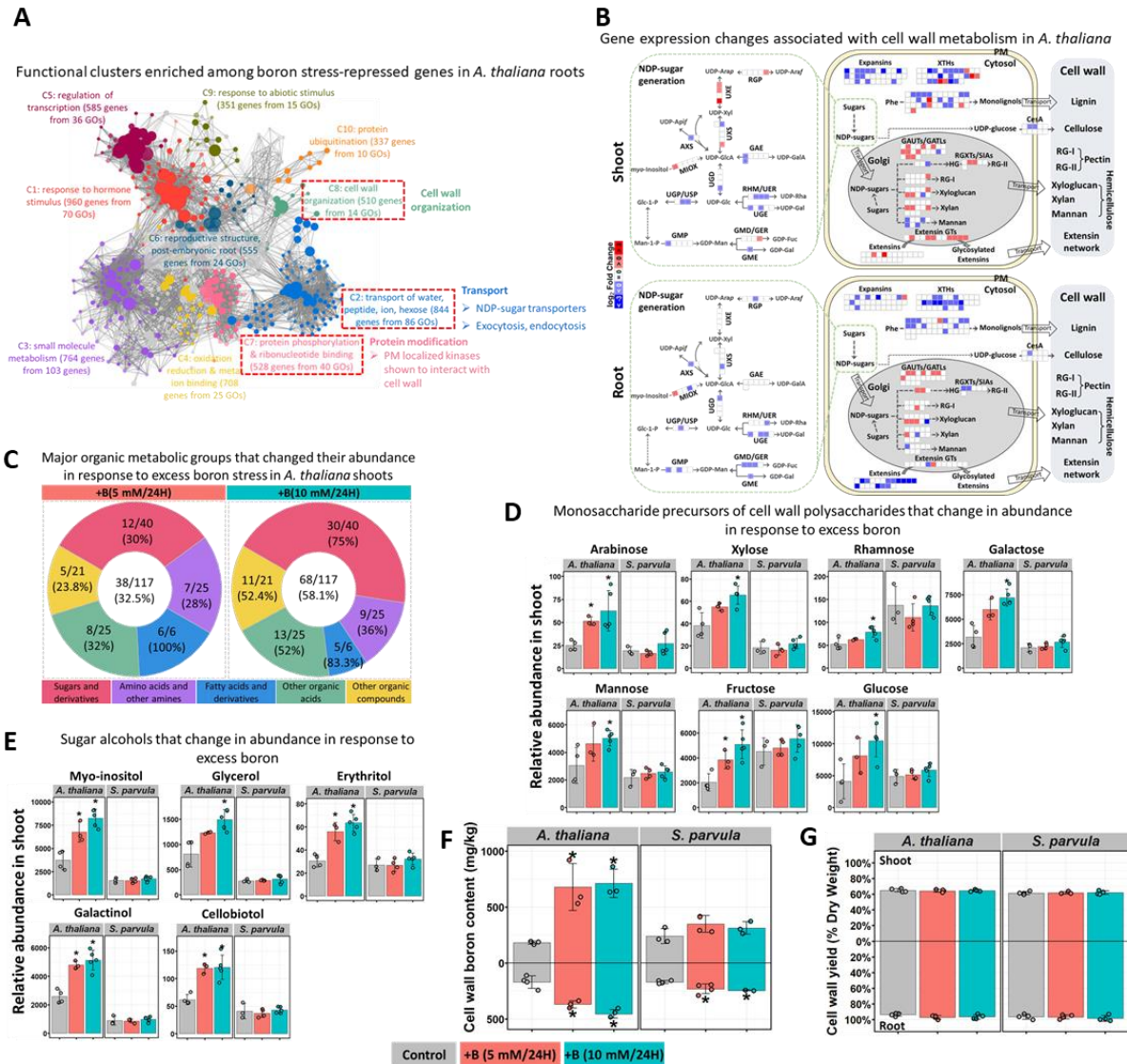
1415

1416

1417

1418

1419



1420

1421 **Figure 3.** Cell wall metabolism is altered under boron toxicity in *A. thaliana*. (A) Functional
 1422 clusters enriched among boron stress-repressed genes in *A. thaliana* roots. Clusters associated
 1423 with cell wall metabolism are marked by red-dashed boxes. Clusters are differently colored and
 1424 labelled with the representative functional term. Each node represents a GO term; node size
 1425 represents genes in the test set assigned to that functional term; GO terms sharing more than 50%
 1426 of genes are connected with edges; and shade of each node represents the *p*-value assigned by the
 1427 enrichment test (FDR-adjusted $p < 0.05$) with darker shades indicating smaller *p*-values. (B)
 1428 Changes in gene expression associated with biosynthesis of cell wall components in response to
 1429 boric acid treatment in *A. thaliana* shoots and roots. Genes are represented by square blocks,
 1430 grouped by families or pathways, with up- and down-regulation marked by red and blue,
 1431 respectively. UDP, uridine diphosphate; UDP-Glc, UDP-glucose; UDP-Gal, UDP-galactose;
 1432 UDP-GlcA, UDP-glucuronic acid; UDP-GalA, UDP-galacturonic acid; UDP-Xyl, UDP-xylose;
 1433 UDP-Ara, UDP-arabinose; UDP-Araf, UDP-arabinofuranose; UDP-Rha, UDP-rhamnose; UDP-
 1434 Api, UDP-apiiose; GDP-Man, GDP-mannose; GDP-Fuc, GDP-fucose; GDP-Gal, GDP-galactose;
 1435 GAE, UDP-D-glucuronic acid 4-epimerase; UXS, UDP-D-xylose synthase; UXE, UDP-D-

1436 xylose 4-epimerase; RGP, reversibly glycosylated protein; AXS, UDP-D-apiose/UDP-D-xylose
1437 synthase (also known as UAXS); MIOX, inositol oxygenase; UGD, UDP-D-glucose
1438 dehydrogenase; UGP/USP, UDP-glucose pyrophosphorylase/UDP-sugar pyrophosphorylase;
1439 RHM/UER, rhamnose synthase gene/ nucleotide-rhamnose epimerase-reductase; UGE, UDP-D-
1440 glucose 4-epimerase; GMP, GDP-D-mannose pyrophosphorylase; GMD/GER, GDP-D-
1441 mannose-4,6-dehydratase/GDP-4-keto-6-deoxy-D-mannose-3,5-epimerase-4-reductase; GME,
1442 GDP-D-mannose 3,5-epimerase; EXTs, extensins; EXT GTs, extensin glycosyltransferases;
1443 EXPs, expansins; XTHs, xyloglucan endotransglucosylase/hydrolases; RGXT,
1444 rhamnogalacturonan xylosyltransferase. (C) Major organic metabolic groups that changed their
1445 abundance in response to excess boron stress in *A. thaliana* shoots. For each category, the
1446 number and proportion of metabolites that changed in abundance compared to the total identified
1447 are shown. (D-E) Monosaccharide precursors of cell wall polysaccharides (D) and sugar alcohols
1448 (E) that changed in abundance in shoots of *A. thaliana* and *S. parvula* 24 hours after boric acid
1449 treatments. The relative abundance is given compared to the internal standard, ribitol. (F) Boron
1450 contents in cell walls extracted from shoots and roots of *A. thaliana* and *S. parvula* under
1451 different treatments for 24 hours. (G) Cell wall yield of shoots and roots in *A. thaliana* and *S.*
1452 *parvula* exposed to different treatments for 24 hours. Cell wall yield was calculated as the
1453 percentage of plant biomass on a dry weight basis. In panels D-G, all values are mean \pm SD
1454 (n=3~5). Asterisks represent significant differences ($p<0.05$) compared to control determined by
1455 Student's t-test.

1456

1457

1458

1459

1460

1461

1462

1463

1464

1465

1466

1467

1468

1469

1470

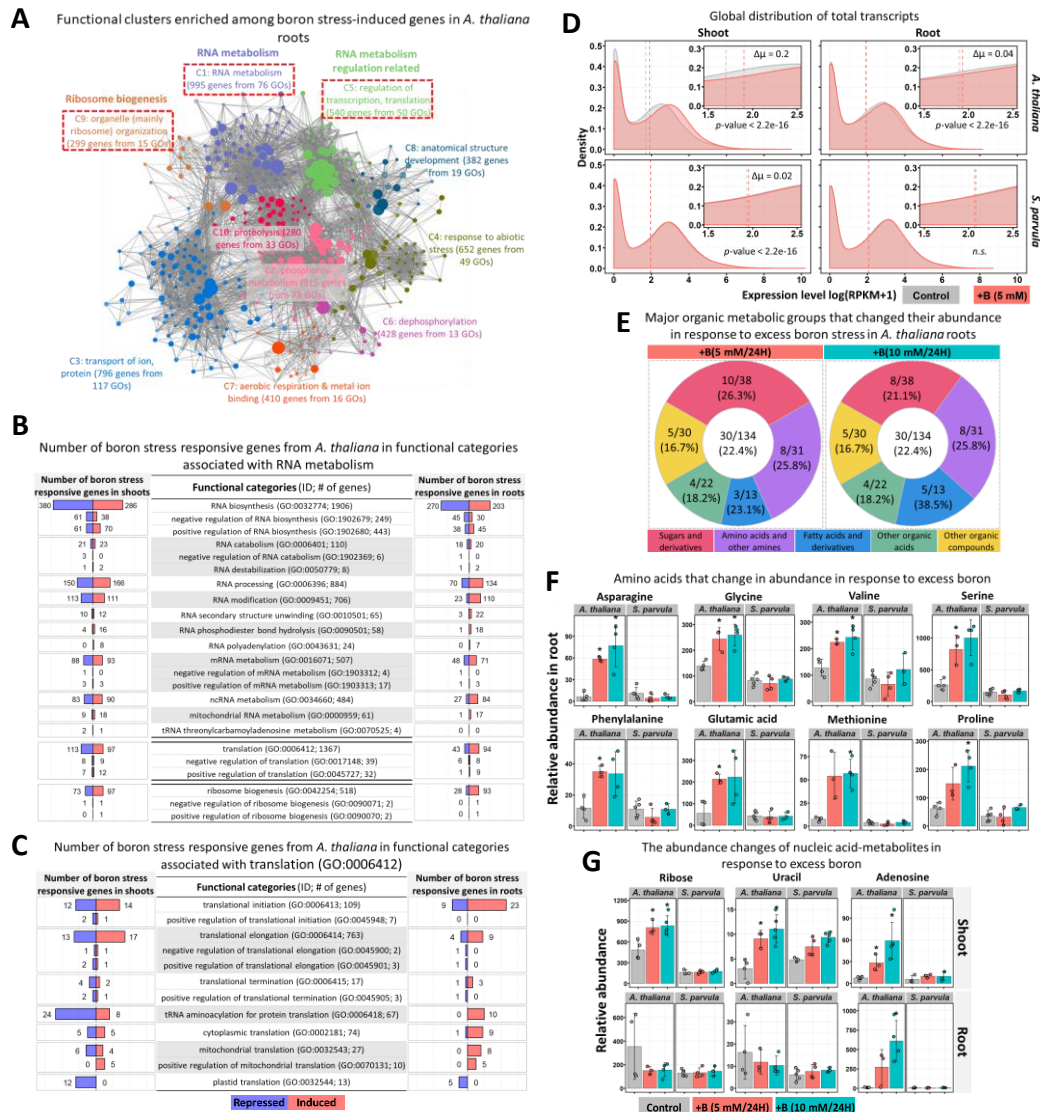


Figure 4. RNA metabolism related processes are affected in response to excess boron in *A. thaliana*. (A) Enriched functional clusters among boron stress-induced genes in *A. thaliana* roots with notable associations for RNA metabolism marked by red-dashed boxes. The network visualization is similar to Figure 3A. (B-C) Number of boron stress responsive genes from *A. thaliana* in functional categories associated with RNA metabolism (B) and translation (GO:0006412). (C). Red and blue indicate up- and down-regulation, respectively. (D) Global transcriptome expression distributions in *A. thaliana* and *S. parvula*. Density distributions of expression in $\log(\text{RPKM}+1)$ for entire transcriptomes were compared to identify transcriptome-wide global changes. p -values were estimated using Wilcoxon signed-rank test. (E) Major organic metabolic groups that changed their abundance in response to excess boron stress in *A. thaliana* roots. For each category, the number and proportion of metabolites that changed in abundance compared to the total identified are shown. (F) Amino acid and (G) nucleic acid-metabolite abundance changes in response to excess boron stress in shoot and root. The relative abundance is given compared to the internal standard, ribitol. Values shown are mean \pm SD ($n = 3, 4$ or 5). Asterisks represent significant differences of each treatment compared to control according to Student's t test ($p < 0.05$).

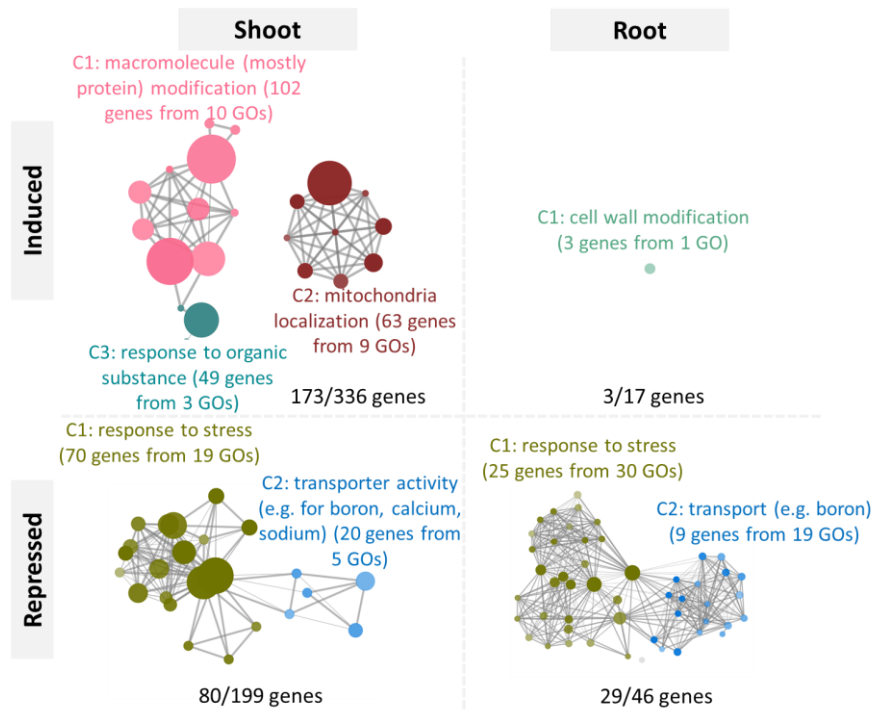


Figure 5. Functional clusters enriched among differentially expressed genes in *S. parvula* in response to excess boron. The network visualization was constructed the same way described for Figure 3A. Numbers assigned for each cluster represent total number of genes from all subclusters/total number of boron stress-responsive genes in the category.

1472

1473

1474

1475

1476

1477

1478

1479

1480

1481

1482

1483

1484

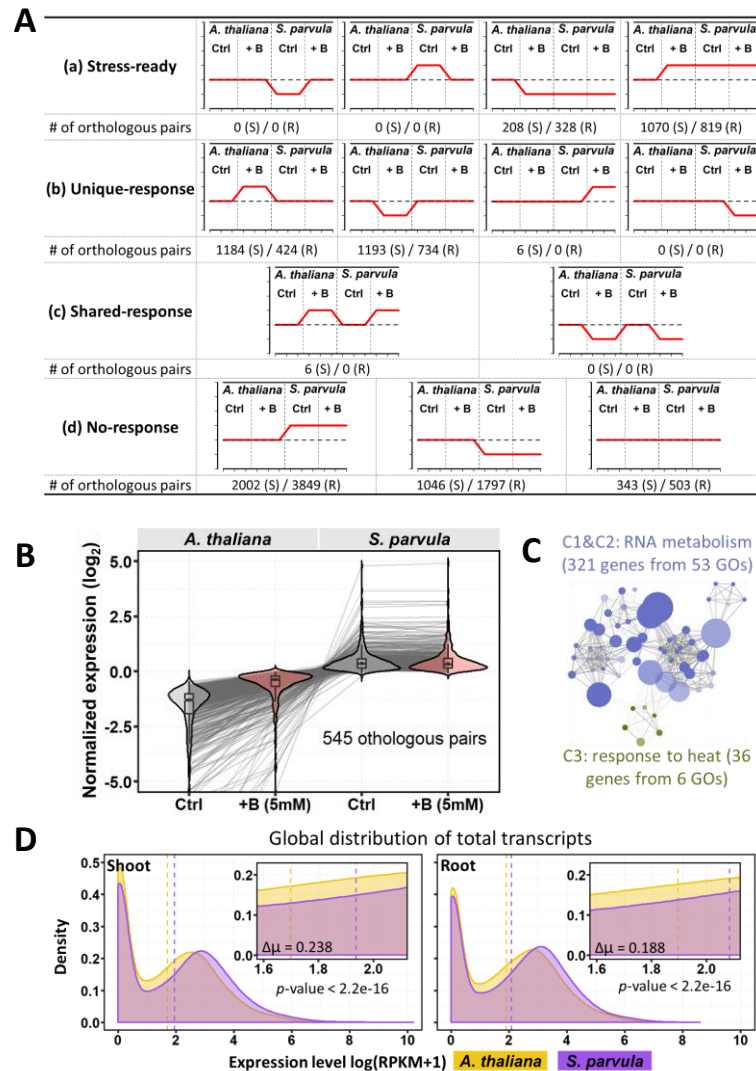


Figure 6. Genes associated with excess boron responses are constitutively expressed in *S. parvula*. (A) Summary of co-expression trends in ortholog pairs between *A. thaliana* and *S. parvula* in response to excess boron. The red lines indicate the trend in expression levels of the ortholog pairs in each species under control and treatment conditions, compared to *A. thaliana* control (dashed line). Ctrl, Control; + B, boric acid treatment; S, Shoot; R, Root. (B) A major co-expression cluster in the “stress-ready” category in (A) that illustrates stress preparedness of the *S. parvula* orthologs in roots (center line, median; box, interquartile range (IQR); notch, $1.5 \times \text{IQR} / \sqrt{n}$; whiskers, $1.5 \times \text{IQR}$). (C) Functional clusters enriched among the ortholog pairs from the example cluster given in (B). The clusters are differently colored and labelled with the representative functions. Node size represents genes in the test set which are annotated to that functional term; edges represent the number of shared genes between functional terms; each cluster is coded with a different color; and shade of each node represents p -value assigned by the enrichment test. Lighter to darker shades indicate larger to smaller p -values, respectively. (D) *S. parvula* shows a higher basal level expression than *A. thaliana*. p -values were estimated using Wilcoxon signed-rank test.

1485

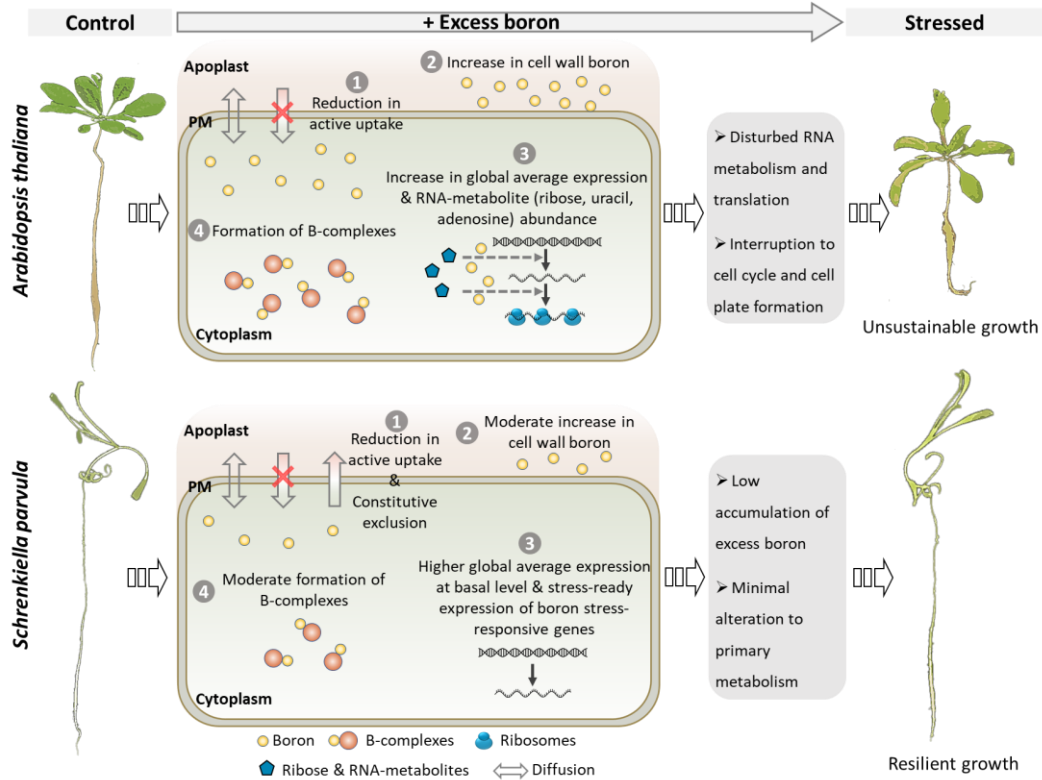


Figure 7. A proposed model for boron toxicity in plants.

1486

1487

1488

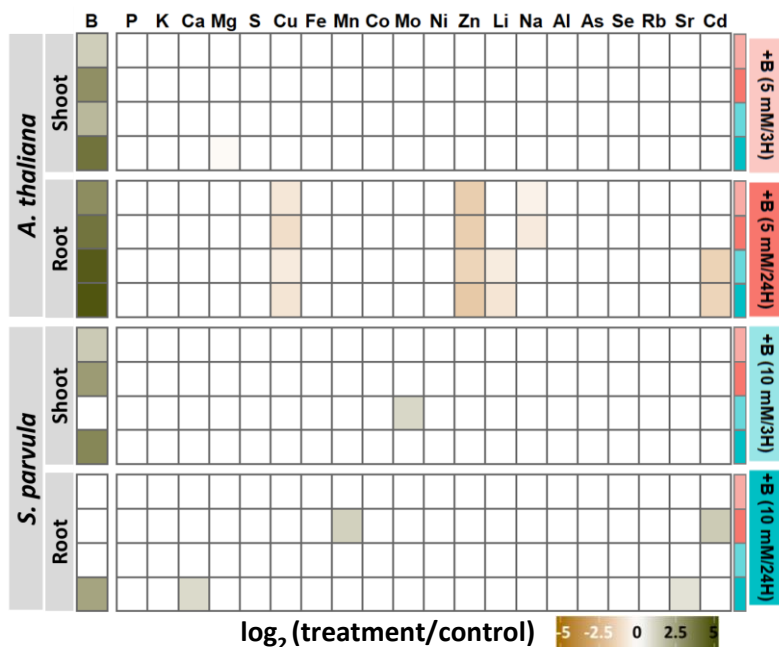
1489

1490

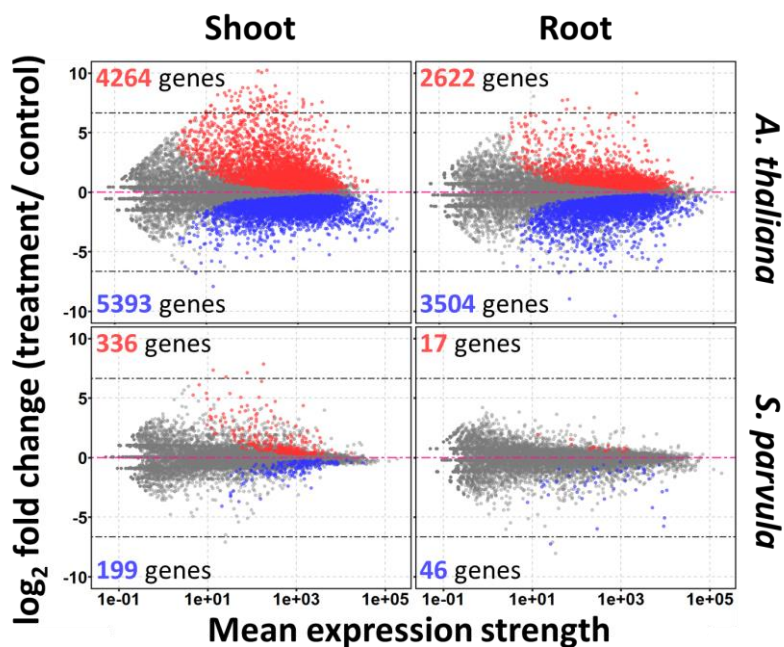
1491

1492

1493



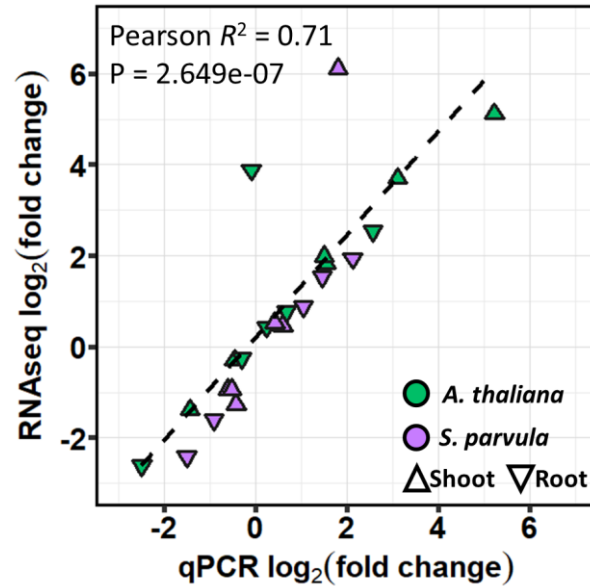
Supplemental Figure 1. Ionomic profiles in response to boric acid treatments. Significant differences of each treatment compared to control were based on one-way ANOVA followed by Tukey's post-hoc tests ($p < 0.05$).



Supplemental Figure 2. Differential expression visualized using MA-plots from shoot (left panel) and root (right panel) of *A. thaliana* (upper panel) and *S. parvula* (lower panel). Red dots represent up-regulated DEGs and blue dots indicate down-regulated DEGs.

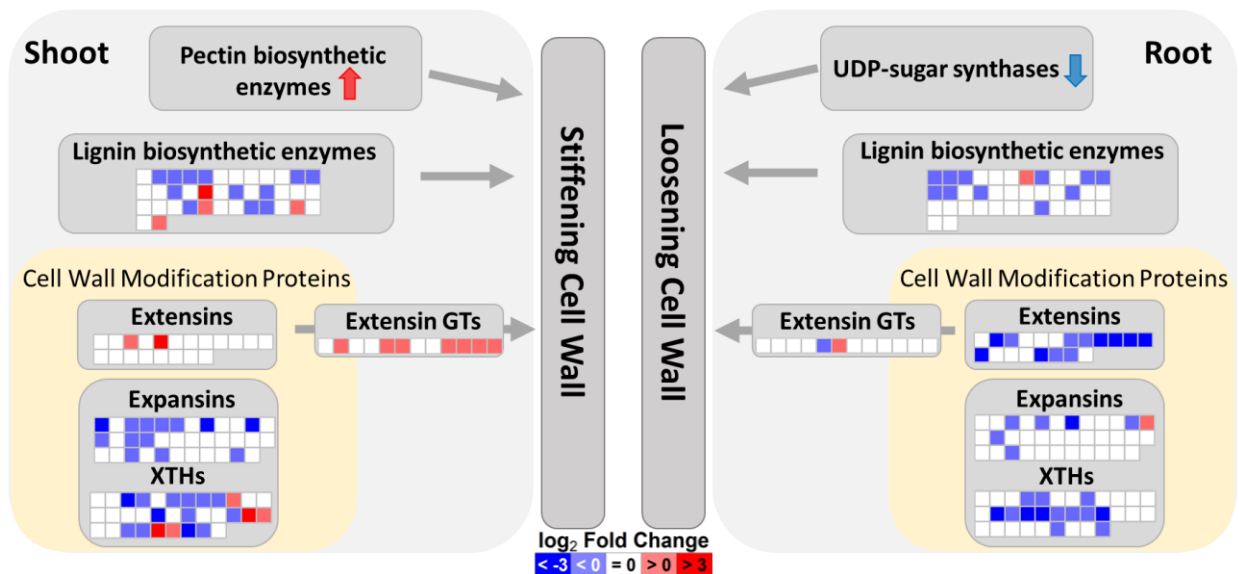
1494

1495



Supplemental Figure 3. Assessment of qPCR and RNA-seq expression data agreement for selected differentially expressed genes.

1496



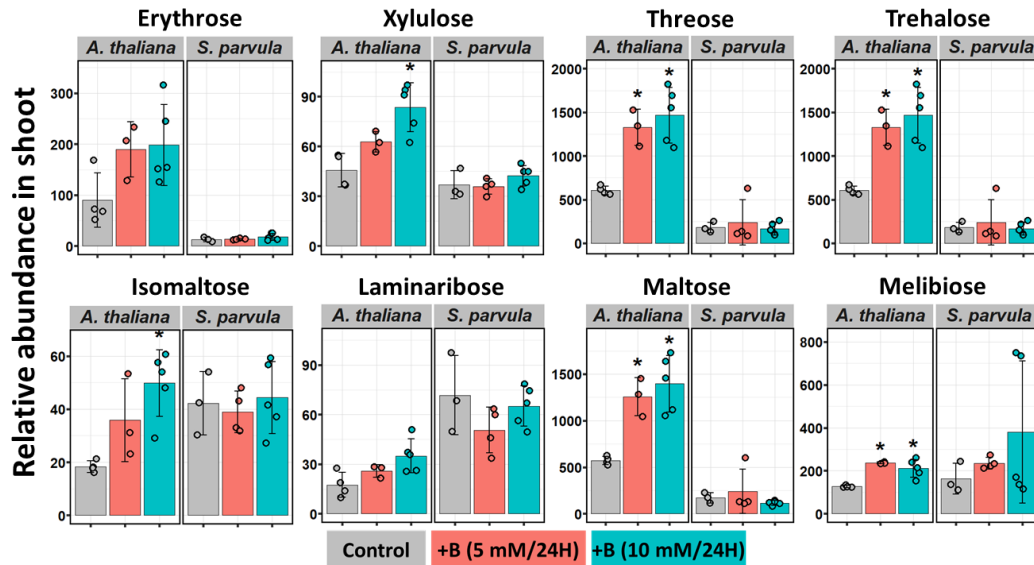
Supplemental Figure 4. Summary of cell wall modifications in *A. thaliana* in response to boric acid treatment. Genes are represented by in colored blocks, grouped into families and pathways, with up- and down-regulation marked by red and blue, respectively.

1497

1498

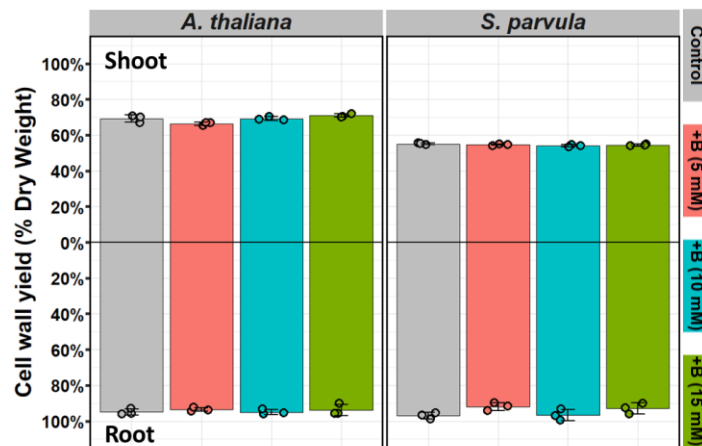
1499

1500



Supplemental Figure 5. Relative abundances of sugars in *A. thaliana* shoots that are not directly associated with cell wall polysaccharides. The relative abundance is given compared to the internal standard, ribitol. Values shown are mean \pm SD (n = 3, 4 or 5). Asterisks represent significant differences of each treatment compared to control according to Student's t test ($p < 0.05$).

1501



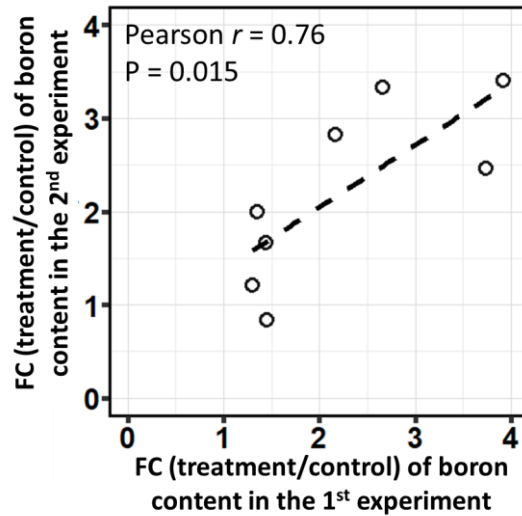
Supplemental Figure 6. Cell wall content in *A. thaliana* and *S. parvula* treated with excess boron for 5 days. Values shown are mean \pm SD (n = 3 or 4).

1502

1503

1504

1505



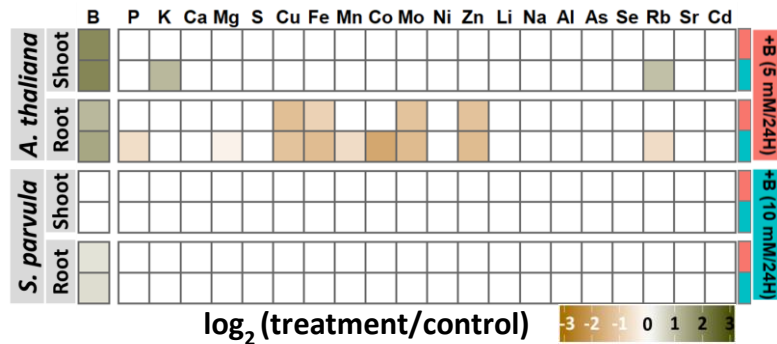
Supplemental Figure 7. Conformance of boron content quantified using two independent experiments. Fold changes were calculated comparing the treatment to the control for each tissue from each species. Pearson’s r and p -values are indicated.

1506

1507

1508

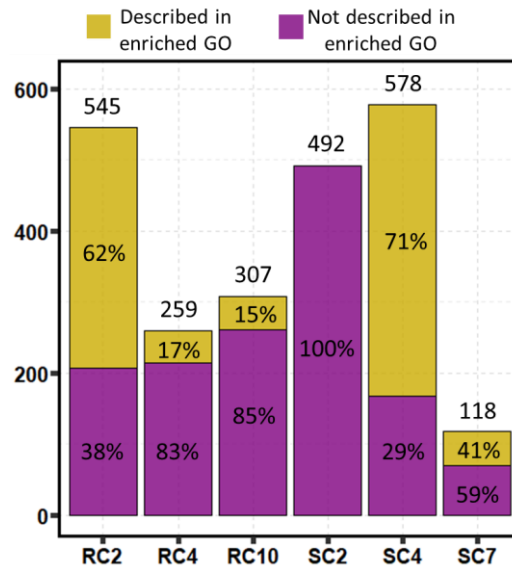
1509



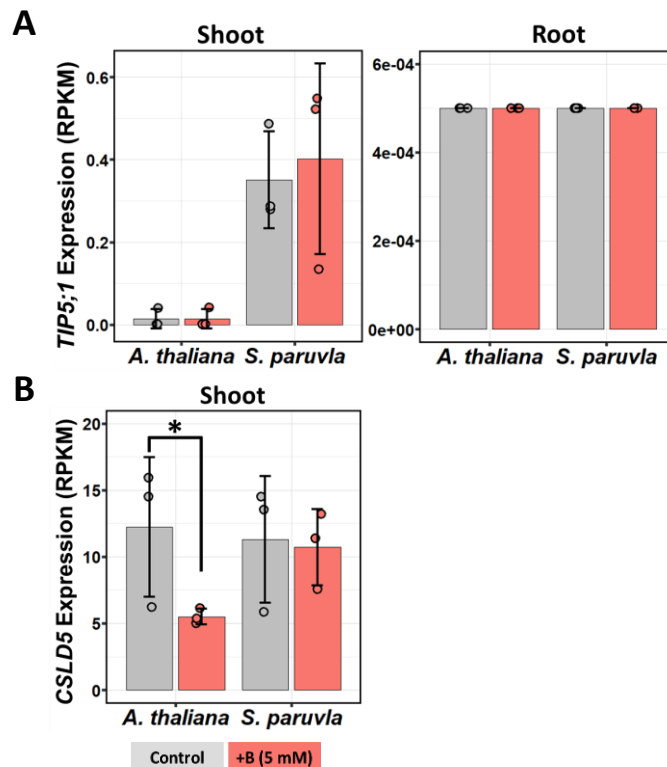
Supplemental Figure 8. Ionic profiles in the cell wall extracts in response to boric acid treatments at 24 hours. Significant differences of each treatment compared to control for each element were based on one-way ANOVA followed by Tukey’s post-hoc tests ($p < 0.05$).

1510

1511

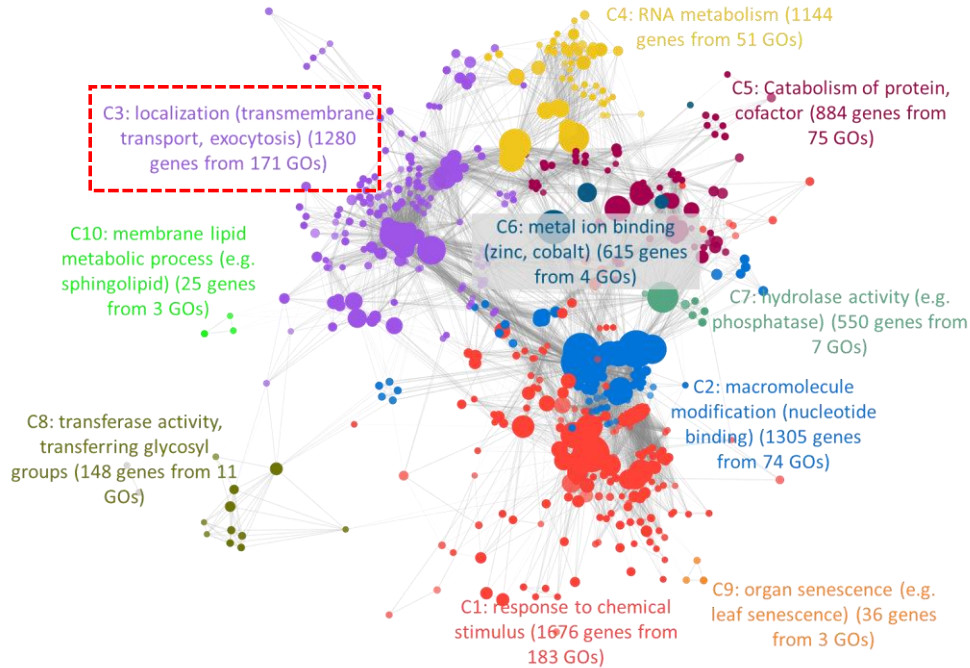


Supplemental Figure 9. Number of members and their annotation availability in selected stress-ready clusters. RC: root cluster; SC: shoot cluster.

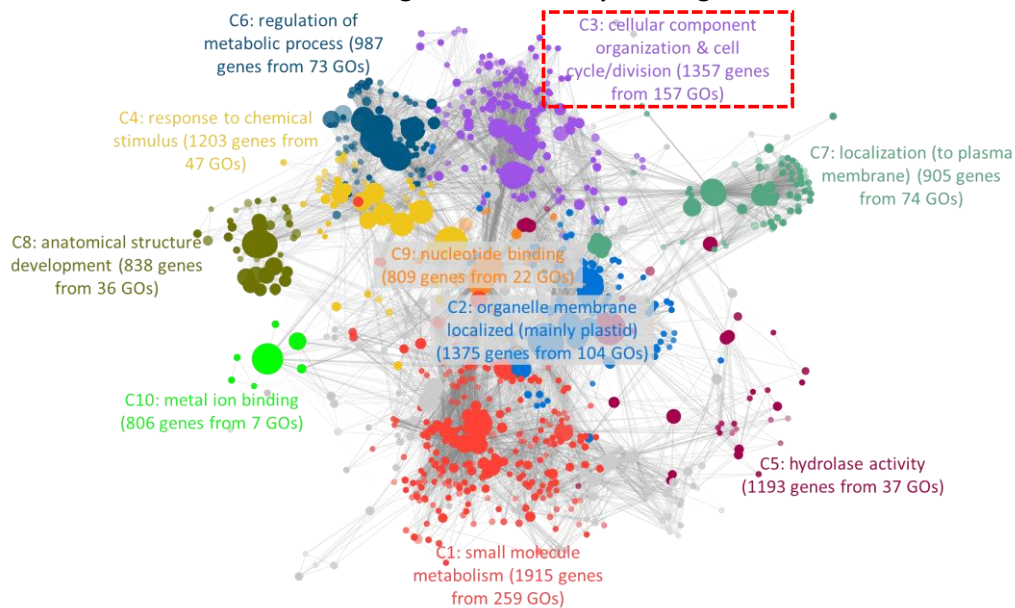


Supplemental Figure 10. Expression levels of *TIP5;1* (A) and *CSLD5* (B) from *A. thaliana* and *S. parvula* in control and 5 mM boric acid treatment. Asterisks represent significant differences in expression compared to control (at FDR-adjusted $p < 0.05$) determined by both DESeq2 and NOISeq.

A Functional clusters enriched among boron stress-induced genes in *A. thaliana* shoots



B Functional clusters enriched among boron stress-repressed genes in *A. thaliana* shoots



Supplemental Figure 11. Functional clusters enriched among genes that were induced (A) and repressed (B) in *A. thaliana* shoots. Top 10 largest clusters are differently colored and labelled with the representative functional terms. Each node represents a GO term; node size represents genes in the test set assigned to that functional term; GO terms sharing more than 50% of genes are connected with edges; and shade of each node represents the p -value assigned by the enrichment test (FDR-adjusted $p < 0.05$) with darker shades indicating smaller p -values.